

1   **An antisense RNA capable of modulating the  
2   expression of the tumor suppressor microRNA-34a**  
3

4   **Jason T. Serviss<sup>1\*</sup>, Felix Clemens Richter<sup>1,2</sup>, Jimmy Van den Eynden<sup>3</sup>,**  
5   **Nathanael Andrews<sup>1</sup>, Miranda Houtman<sup>1,4</sup>, Mattias Vesterlund<sup>1</sup>, Laura**  
6   **Schwarzmueller<sup>1,5</sup>, Per Johnsson<sup>6,7</sup>, Erik Larsson<sup>3</sup>, Dan Grandér<sup>1</sup>, Katja**  
7   **Pokrovskaia Tamm<sup>1</sup>**

8                   <sup>1</sup> Department of Oncology and Pathology, Karolinska Institutet, Stockholm, Sweden, SE-  
9                   17177

10                 <sup>2</sup> Kennedy Institute of Rheumatology, University of Oxford, Roosevelt Drive, Oxford OX3 7FY,  
11                 UK

12                 <sup>3</sup> Department of Medical Biochemistry and Cell Biology, Institute of Biomedicine, The  
13                 Sahlgrenska Academy, University of Gothenburg, SE-405 30 Gothenburg, Sweden

14                 <sup>4</sup> Rheumatology Unit, Department of Medicine, Karolinska University Hospital, Solna,  
15                 Karolinska Institutet, Stockholm, Sweden

16                 <sup>5</sup> Laboratory for Experimental Oncology and Radiobiology (LEXOR), Center for Experimental  
17                 Molecular Medicine (CEMM), Academic Medical Center, Amsterdam, The Netherlands

18                 <sup>6</sup> Ludwig Institute for Cancer Research, Stockholm, Sweden

19                 <sup>7</sup> Department of Cell and Molecular Biology, Karolinska Institutet, Stockholm, Sweden

20                 **\* Correspondence:**

21                 Jason T. Serviss [jason.serviss@ki.se](mailto:jason.serviss@ki.se)

22                 **Abstract**

23                 The microRNA-34a is a well-studied tumor suppressor microRNA (miRNA)  
24                 and a direct downstream target of TP53 with roles in several pathways  
25                 associated with oncogenesis, such as proliferation, cellular growth, and  
26                 differentiation. Due to its broad tumor suppressive activity, it is not surprising  
27                 that *miR34a* expression is altered in a wide variety of solid tumors and  
28                 hematological malignancies. However, the mechanisms by which *miR34a* is  
29                 regulated in these cancers is largely unknown. In this study, we find that a  
30                 long non-coding RNA transcribed antisense to the *miR34a* host gene, is  
31                 critical for *miR34a* expression and mediation of its cellular functions in multiple  
32                 types of human cancer. We name this long non-coding RNA *lncTAM34a*, and  
33                 characterize its ability to facilitate *miR34a* expression under different types of  
34                 cellular stress in both *TP53* deficient and wildtype settings.

40

41 **Introduction**

42 In recent years advances in functional genomics have revolutionized our  
43 understanding of the human genome. Evidence now points to the fact that  
44 approximately 75% of the genome is transcribed but only ~1.2% of this is  
45 responsible for encoding proteins (International Human Genome Sequencing  
46 2004, Djebali et al. 2012). Of these recently identified elements, long non-  
47 coding (lnc) RNAs are defined as transcripts exceeding 200 base pairs (bp) in  
48 length with a lack of a functional open reading frame. Some lncRNAs are  
49 dually classified as antisense (as) RNAs that are expressed from the same  
50 locus as a sense transcript in the opposite orientation. Current estimates  
51 using high-throughput transcriptome sequencing, indicate that up to 20-40%  
52 of the approximately 20,000 protein-coding genes exhibit antisense  
53 transcription (Chen et al. 2004, Katayama et al. 2005, Ozsolak et al. 2010).

54 Systematic large-scale studies have shown aberrant expression of asRNAs to  
55 be associated with tumorigenesis (Balbin et al. 2015) and, although  
56 characterization of several of these has identified asRNA-mediated regulation  
57 of multiple well known tumorigenic factors (Yap et al. 2010, Johnsson et al.  
58 2013), the vast majority of potential tumor-associated lncRNAs have not yet  
59 been characterized. The known mechanisms by which asRNAs accomplish  
60 their regulatory functions are diverse, and include recruitment of chromatin  
61 modifying factors (Rinn et al. 2007, Johnsson et al. 2013), acting as  
62 microRNA (miRNA) sponges (Memczak et al. 2013), and causing  
63 transcriptional interference (Conley et al. 2012).

64

65 Responses to cellular stress, e.g. DNA damage, sustained oncogene  
66 expression, and nutrient deprivation, are all tightly controlled cellular pathways  
67 that are almost universally dysregulated in cancer. Cellular signaling, in  
68 response to these types of stresses, often converges on the transcription  
69 factor TP53 that regulates transcription of coding and non-coding downstream  
70 targets. One important non-coding target of TP53 is the tumor suppressor  
71 microRNA known as *miR34a* (Raver-Shapira et al. 2007).  
72 Upon TP53 activation *miR34a* expression is increased allowing it to down-  
73 regulate target genes involved in cellular pathways such as growth factor  
74 signaling, apoptosis, differentiation, and cellular senescence (Lal et al. 2011,  
75 Slabakova et al. 2017). Thus, *miR34a* is a crucial factor in mediating activated  
76 TP53 response and, the fact that it is often deleted or down-regulated in  
77 human cancers indicates, its tumor suppressive effect and makes it a valuable  
78 prognostic marker (Cole et al. 2008, Gallardo et al. 2009, Zenz et al. 2009,  
79 Cheng et al. 2010, Liu et al. 2011). Reduced *miR34a* transcription is mediated  
80 via epigenetic regulation in many solid tumors, including colorectal-,  
81 pancreatic-, and ovarian cancer (Vogt et al. 2011), as well as numerous types  
82 of hematological malignancies (Chim et al. 2010). In addition, *miR34a* has  
83 been shown to be transcriptionally regulated via TP53 homologs, TP63 and  
84 TP73, other transcription factors, e.g. STAT3 and MYC, and, in addition, post-  
85 transcriptionally through miRNA sponging by the NEAT1 lncRNA (Chang et al.  
86 2008, Su et al. 2010, Agostini et al. 2011, Rokavec et al. 2015, Ding et al.  
87 2017). Despite these findings, the mechanisms underlying *miR34a* regulation  
88 in the context of oncogenesis have not yet been fully elucidated.

89

90 Studies across multiple cancer types have reported a decrease in oncogenic  
91 phenotypes when *miR34a* expression is induced in a *TP53*-null background,  
92 although endogenous mechanisms for achieving this have not yet been  
93 discovered (Liu et al. 2011, Ahn et al. 2012, Yang et al. 2012, Stahlhut et al.  
94 2015, Wang et al. 2015). In addition, previous reports from large-scale studies  
95 interrogating global *TP53*-mediated regulation of lncRNAs have identified a  
96 lncRNA (known as RP3-510D11.2 and LINC01759) originating in the  
97 antisense orientation from the *miR34a* locus which is induced upon numerous  
98 forms of cellular stress (Rashi-Elkeles et al. 2014, Hunten et al. 2015, Leveille  
99 et al. 2015, Ashouri et al. 2016, Kim et al. 2017). Despite this, none of these  
100 studies have functionally characterized this transcript, which we name Long-  
101 Non-coding Transcriptional Activator of *MiR34a* (lncTAM34a). In this study we  
102 functionally characterize the *lncTAM34a* transcript, and find that it positively  
103 regulates *miR34a* expression resulting in a decrease of several tumorigenic  
104 phenotypes. Furthermore, we find that *lncTAM34a*-mediated up-regulation of  
105 *miR34a* is sufficient to induce endogenous cellular mechanisms counteracting  
106 several types of stress stimuli in a *TP53*-deficient background. Finally, similar  
107 to the functional roles of antisense transcription at protein-coding genes, we  
108 identify a rare example of an antisense RNA capable of regulating a cancer-  
109 associated miRNA.

110

## 111 **Results**

112

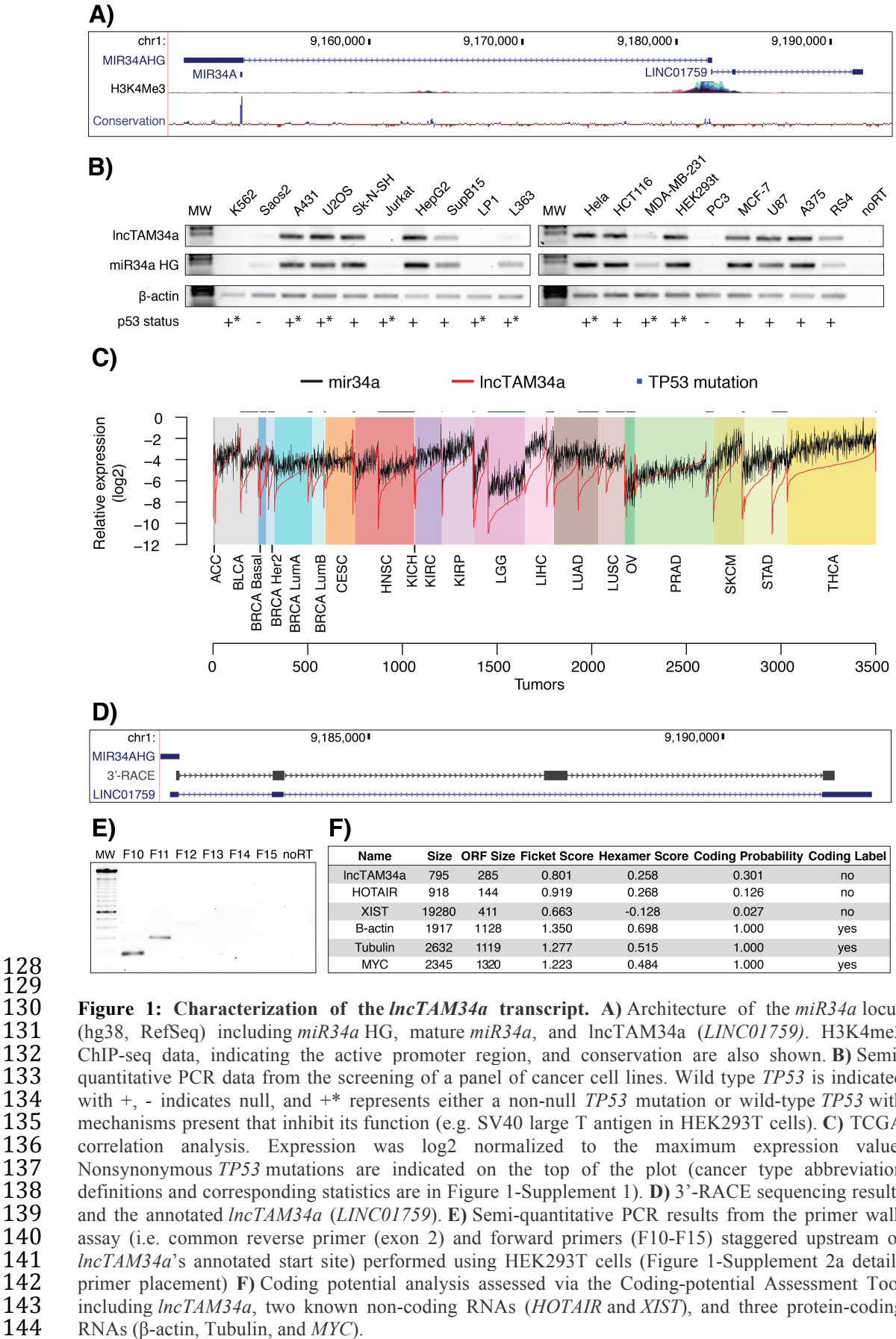
113 ***lncTAM34a* is a broadly expressed non-coding transcript whose levels**  
114 **correlate with *miR34a* expression**

115

116 *lncTAM34a* is transcribed in a “head-to-head” orientation with approximately  
117 100 base pair overlap with the *miR34a* host gene (HG) (**Fig. 1a**). Due to the

fact that sense/antisense pairs can be both concordantly and discordantly expressed, we sought to evaluate this relationship in the case of *miR34a* HG and its asRNA. Using a diverse panel of cancer cell lines, we detected co-expression of both the *miR34a* HG and *lncTAM34a* (**Fig. 1b**). We used cell lines with a known *TP53* status in the panel due to previous reports that *miR34a* is a known downstream target of *TP53*. These results indicate that *miR34a* HG and *lncTAM34a* are co-expressed and that their expression levels correlate with *TP53* status, with *TP53*<sup>-/-</sup> cells tending to have decreased or undetectable expression of both transcripts.

127



145 We next sought to analyze primary cancer samples to examine whether a  
146 correlation between *lncTAM34a* and *miR34a* expression levels could be  
147 identified. We utilized RNA sequencing data from The Cancer Genome Atlas  
148 (TCGA) after stratifying patients by cancer type, *TP53* status, and, in the case  
149 of breast cancer, cancer subtypes. The results indicate that *lncTAM34a*  
150 and *miR34a* expression are strongly correlated in the vast majority of cancer  
151 types examined, both in the presence and absence of wild-type *TP53* (**Fig.**  
152 **1c, Figure 1-Figure Supplement 1a**). The results also further confirm that  
153 the expression levels of both *miR34a* and *lncTAM34a* are significantly  
154 reduced in patients with nonsynonymous *TP53* mutations (**Figure 1-Figure**  
155 **Supplement 1b**).

156

157 Next, we aimed to gain a thorough understanding of *lncTAM34a*'s molecular  
158 characteristics and cellular localization. To experimentally determine the 3'  
159 termination site for the *lncTAM34a* transcript we performed 3' rapid  
160 amplification of cDNA ends (RACE) using the U2OS osteosarcoma cell line  
161 that exhibited high endogenous levels of *lncTAM34a* in the cell panel  
162 screening. Sequencing the cloned cDNA indicated that the transcripts 3'  
163 transcription termination site is 525 base pairs upstream of  
164 the *lncTAM34a* transcript's annotated termination site (**Fig. 1d**). Next, we  
165 characterized the *lncTAM34a* 5' transcription start site by carrying out a  
166 primer walk assay, i.e. a common reverse primer was placed in exon 2 and  
167 forward primers were gradually staggered upstream of *lncTAM34a*'s  
168 annotated start site (**Figure 1-Figure Supplement 2a**). Our results indicated  
169 that the 5' start site for *lncTAM34a* is in fact approximately 90bp (F11 primer)

170 to 220bp (F12 primer) upstream of the annotated start site (**Fig. 1e**).  
171 Polyadenylation status was evaluated via cDNA synthesis with either random  
172 nanomers or oligo(DT) primers followed by semi-quantitative PCR which  
173 showed that the *lncTAM34a* is polyadenylated although the unspliced form  
174 seems to only be present in a polyadenylation negative state (**Figure 1-**  
175 **Figure Supplement 2b**). Furthermore, we investigated the propensity  
176 of *lncTAM34a* to be alternatively spliced in U2OS cells, using PCR cloning  
177 followed by sequencing and found that the transcript is post-transcriptionally  
178 spliced to form multiple isoforms (**Figure 1-Figure Supplement 2c**). In order  
179 to evaluate the subcellular localization of *lncTAM34a*, we made use of RNA  
180 sequencing data from five cancer cell lines included in the ENCODE  
181 (Consortium 2012) project that had been fractionated into cytosolic and  
182 nuclear fractions. The analysis revealed that the *lncTAM34a* transcript  
183 primarily localizes to the nucleus with only a minor fraction in the cytosol  
184 (**Figure 1-Figure Supplement 2d**).

185  
186 Lastly, we utilized several approaches to evaluate the coding potential of  
187 the *lncTAM34a* transcript. The Coding-Potential Assessment Tool is a  
188 bioinformatics-based tool that uses a logistic regression model to evaluate  
189 coding-potential by examining open reading frame (ORF) length, ORF  
190 coverage, Fickett score, and hexamer score (Wang et al. 2013). Results  
191 indicated that *lncTAM34a* has a similar low coding capacity to known non-  
192 coding transcripts such as HOTAIR and XIST (Fig. 1F). We further confirmed  
193 these results using the Coding-Potential Calculator that uses a support vector  
194 machine-based classifier and accesses an alternate set of discriminatory

195 features (**Figure 1-Figure Supplement 2e**) (Kong et al. 2007). Finally, we  
196 downloaded mass spectrometry spectra for 11 cancer cell lines (Geiger et al.  
197 2012), 7 of which were also present in the cell line panel above (**Fig. 1b**), and  
198 searched it against a database of human protein sequences which also  
199 contained the 6 frame translation of *IncTAM34a*. However, we did not manage  
200 to detect any peptides matching the sequence in any of the 11 cell lines.  
201 Taken together our results indicate that *IncTAM34a* is not a coding transcript  
202 and that it is not translated to any significant degree.

203

#### 204 **TP53-mediated regulation of *IncTAM34a* expression**

205 *miR34a* is a known downstream target of TP53 and has been previously  
206 shown to exhibit increased expression within multiple contexts of cellular  
207 stress. *IncTAM34a* has also been shown to be induced upon TP53 activation  
208 in several global analyses of TP53-regulated lncRNAs (Rashi-Elkeles et al.  
209 2014, Hunten et al. 2015, Leveille et al. 2015, Ashouri et al. 2016, Kim et al.  
210 2017). To confirm these results in our biological systems, we treated  
211 HEK293T, embryonic kidney cells, and HCT116, colorectal cancer cells, with  
212 the DNA damaging agent doxorubicin to activate TP53. QPCR-mediated  
213 measurements of both *miR34a* HG and asRNA indicated that their expression  
214 levels were increased in response to doxorubicin treatment in both cell lines  
215 (**Fig. 2a**). To assess whether TP53 was responsible for the increase  
216 in *IncTAM34a* expression upon DNA damage, we treated *TP53<sup>+/+</sup>* and *TP53<sup>-/-</sup>*  
217 HCT116 cells with increasing concentrations of doxorubicin and monitored the  
218 expression of both *miR34a* HG and *IncTAM34a*. We observed a dose-  
219 dependent increase in both *miR34a* HG and *IncTAM34a* expression levels

220 with increasing amounts of doxorubicin, revealing that these two transcripts  
221 are co-regulated, although, this effect was largely abrogated in *TP53*<sup>-/-</sup> cells  
222 (**Fig. 2b**). These results indicate that TP53 activation increases *lncTAM34a*  
223 expression upon DNA damage. Nevertheless, *TP53*<sup>-/-</sup> cells also showed a  
224 dose-dependent increase in both *miR34a* HG and asRNA, suggesting that  
225 additional factors, other than *TP53* are capable of initiating an increase in  
226 expression of both of these transcripts upon DNA damage.

227

228  
229  
230  
231  
232  
233  
234  
235  
236  
237  
238  
239  
240  
241

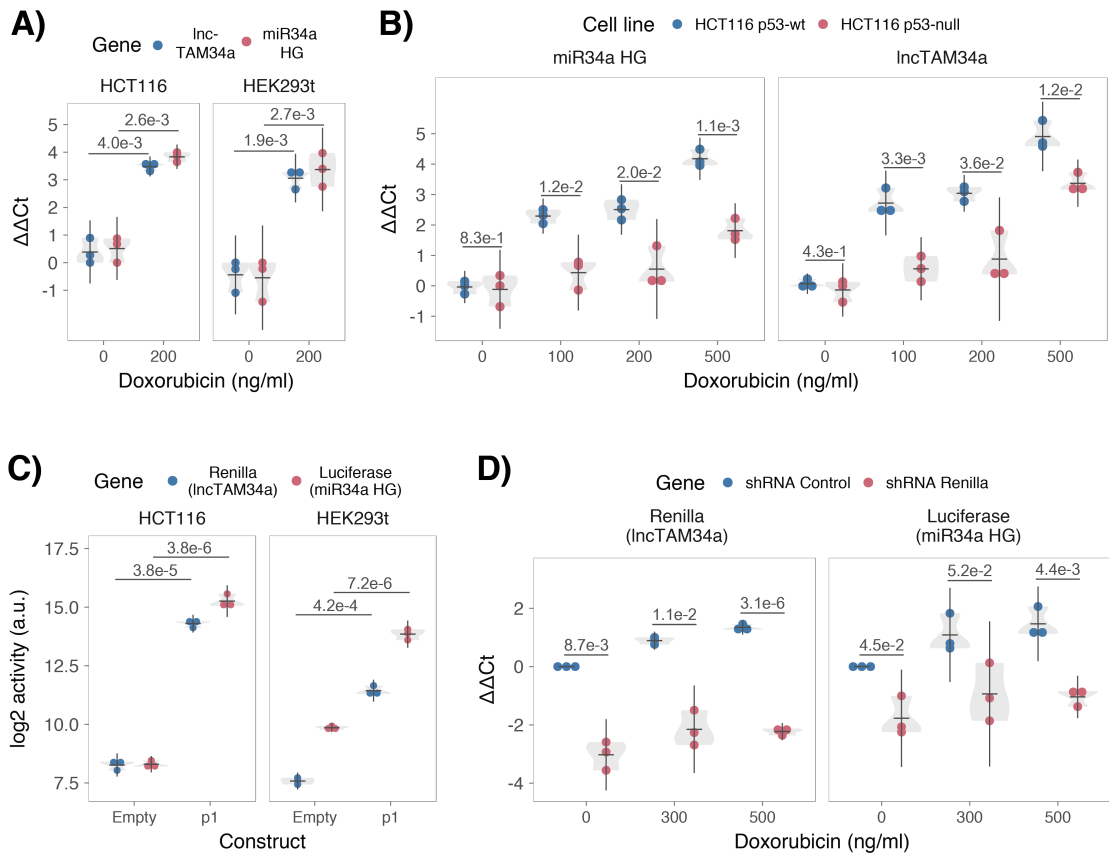


**Figure 2: TP53-mediated regulation of the *miR34a* locus.** **A)** Evaluating the effects of 24 hours of treatment with 200 ng/ml doxorubicin on *LncTAM34a* and *miR34a* HG in HCT116 and HEK293T cells.\* **B)** Monitoring *miR34a* HG and *LncTAM34a* expression levels during 24 hours of doxorubicin treatment in *TP53*<sup>+/+</sup> and *TP53*<sup>-/-</sup> HCT116 cells.\* **C)** Quantification of luciferase and renilla levels after transfection of HCT116 and HEK293T cells with the p1 construct (Figure 2-Supplement 2 contains a schematic representation of the p1 construct).\* **D)** HCT116 cells were co-transfected with the p1 construct and shRNA renilla or shRNA control and subsequently treated with increasing doses of doxorubicin. 24 hours post-treatment, cells were harvested and renilla and luciferase levels were measured using QPCR.\* Individual points represent results from independent experiments and the gray shadow indicates the density of those points. Error bars show the 95% CI, black horizontal lines represent the mean, and P values are shown over long horizontal lines indicating the comparison tested. All experiments in Figure 2 were performed in biological triplicate.

242 The head-to-head orientation of *miR34a* HG and *lncTAM34a*, suggests that  
243 transcription is initiated from a single promoter in a bi-directional manner (**Fig**  
244 **1a**). To investigate whether *miR34a* HG and *lncTAM34a* are transcribed from  
245 the same promoter as divergent transcripts, we cloned the previously reported  
246 *miR34a* HG promoter, including the TP53 binding site, into a luciferase/renilla  
247 dual reporter vector which we hereafter refer to as p1 (**Figure 2-Figure**  
248 **Supplement 1a-b**) (Raver-Shapira et al. 2007). Upon transfection of p1 into  
249 HCT116 and HEK293T cell lines we observed increases in both luciferase  
250 and renilla indicating that *miR34a* HG and *lncTAM34a* expression can be  
251 regulated by a single promoter contained within the p1 construct (**Fig. 2c**).  
252

253 ***lncTAM34a* facilitates miR34a induction in response to DNA damage**  
254 We hypothesized that *lncTAM34a* may regulate *miR34a* HG levels and, in  
255 addition, that the overlapping regions of the sense and antisense transcripts  
256 may mediate this regulation. Knockdown of endogenous *lncTAM34a* is  
257 complicated by its various isoforms (**Figure 1-Figure Supplement 2c**). For  
258 this reason, we utilized the p1 construct to evaluate the regulatory role of  
259 *lncTAM34a* on *miR34a* HG. Accordingly, we first co-transfected the p1  
260 construct, containing the overlapping region of the two transcripts, and two  
261 different short hairpin (sh) RNAs targeting renilla into HEK293T cells and  
262 subsequently measured luciferase and renilla expression. The results  
263 indicated that shRNA-mediated knock-down of the p1-renilla transcript  
264 (corresponding to *lncTAM34a*) caused p1-luciferase (corresponding  
265 to *miR34a* HG) levels to concomitantly decrease (**Figure 2-Figure**  
266 **Supplement 2**). The results suggest that *lncTAM34a* positively regulates

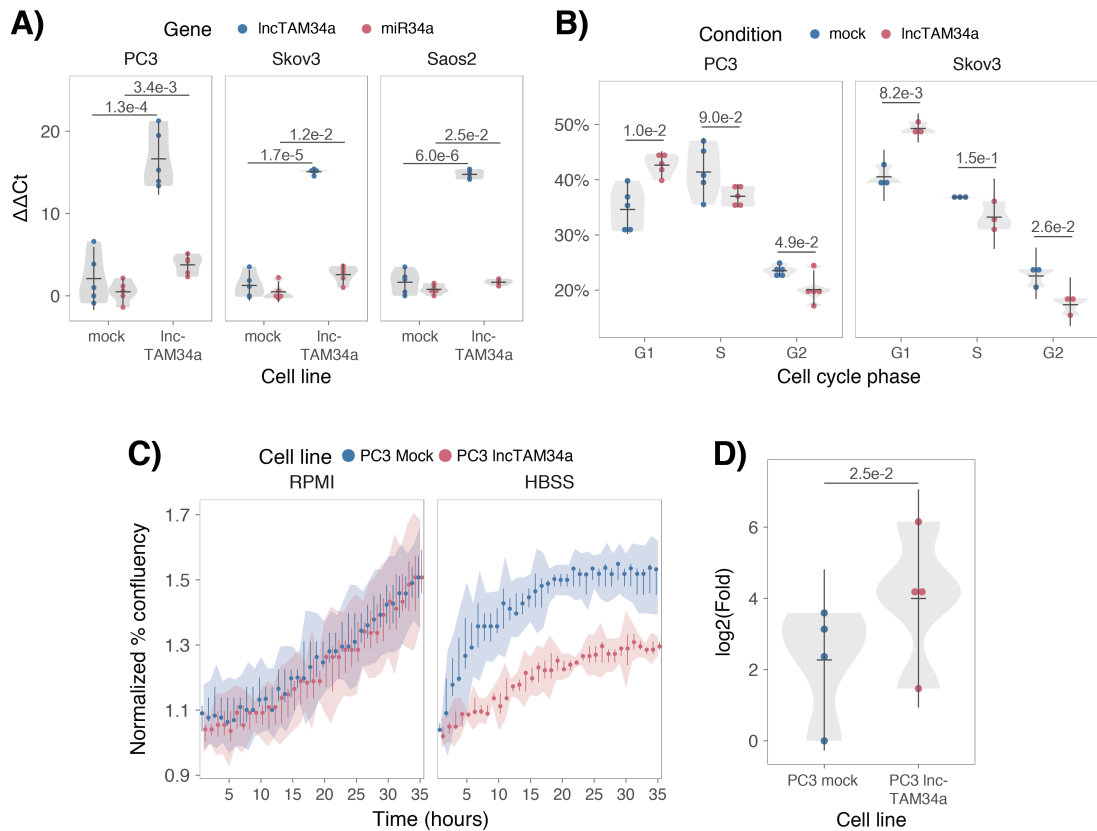
267 levels of *miR34a* HG and that the transcriptional product of *lncTAM34a* within  
268 the p1 construct contributes to inducing a *miR34a* response. To further  
269 support these conclusions and better understand the role of *lncTAM34a*  
270 during TP53 activation, *TP53<sup>+/+</sup>* HCT116 cells were co-transfected with p1  
271 and shRNA renilla (2.1) and subsequently treated with increasing doses of  
272 doxorubicin. Again, the results showed a concomitant reduction in luciferase  
273 levels upon knock-down of p1-renilla i.e. the *lncTAM34a* corresponding  
274 segment of the p1 transcript (**Fig. 2d**). Furthermore, the results showed that in  
275 the absence of p1-renilla the expected induction of p1-luciferase in response  
276 to TP53 activation by DNA damage is abrogated. Collectively these results  
277 indicate that *lncTAM34a* positively regulates *miR34a* expression and  
278 furthermore, suggests that it is crucial for an appropriate TP53-  
279 mediated *miR34a* response to DNA damage.

280

### 281 ***lncTAM34a* can regulate *miR34a* host gene independently of TP53**

282 Despite the fact that TP53 regulates *miR34a* HG and asRNA expression, our  
283 results showed that other factors are also able to regulate this locus (**Fig. 2b**).  
284 Utilizing a lentiviral system, we stably over-expressed the *lncTAM34a*  
285 transcript in three *TP53*-null cell lines, PC3 (prostate cancer), Saos2  
286 (osteogenic sarcoma), and Skov3 (ovarian adenocarcinoma). We first  
287 analyzed the levels of *lncTAM34a* in these stable cell lines, compared to  
288 HEK293T cells, which have high endogenous levels of *lncTAM34a*. On  
289 average, the over-expression was approximately 30-fold higher in the over-  
290 expression cell lines than in HEK293T cells, roughly corresponding to  
291 physiologically relevant levels in cells encountering a stress stimulus, such as

292 DNA damage (**Figure 3-Figure Supplement 1**). Analysis of *miR34a* levels in  
293 the *lncTAM34a* over-expressing cell lines showed that this over-expression  
294 resulted in a concomitant increase in the expression of *miR34a* in all three cell  
295 lines (**Fig. 3a**). These results indicate that, in the absence of  
296 *TP53*, *miR34a* expression may be rescued by activating *lncTAM34a*  
297 expression.



298

299 **Figure 3: *IncTAM34a* positively regulates *miR34a* and its associated phenotypes.** A) QPCR-  
300 mediated quantification of *miR34a* expression in cell lines stably over-expressing *IncTAM34a*.\* B)  
301 Cell cycle analysis comparing stably over-expressing *IncTAM34a* cell lines to the respective mock  
302 control.\* C) Analysis of cellular growth over time in *IncTAM34a* over-expressing PC3 cells. Points  
303 represent the median from 3 independent experiments, the colored shadows indicate the 95%  
304 confidence interval, and vertical lines show the minimum and maximum values obtained from the three  
305 experiments. D) Differential phosphorylated polymerase II binding in *IncTAM34a* over-expressing PC3  
306 cells.\* Individual points represent results from independent experiments and the gray shadow  
307 indicates the density of those points. Error bars show the 95% CI, black horizontal lines represent the  
308 mean, and P values are shown over long horizontal lines indicating the comparison tested.  
309

310 *miR34a* has been previously shown to regulate cell cycle progression, with  
311 *miR34a* induction causing G1 arrest (Raver-Shapira et al. 2007, Tarasov et al.  
312 2007). Cell cycle analysis via determination of DNA content showed a  
313 significant increase in G1 phase cells and a concomitant decrease in G2  
314 phase cells in the PC3 and Skov3 *lncTAM34a* over-expressing cell lines,  
315 indicating G1 arrest (**Fig. 3b**). The effects of *miR34a* on the cell cycle are  
316 mediated by its ability to target cell cycle regulators such as cyclin D1  
317 (*CCND1*) (Sun et al. 2008). Quantification of both *CCND1* RNA expression  
318 (**Figure 3-Figure Supplement 2a**) and protein levels (**Figure 3-Figure**  
319 **Supplement 2b**) in the PC3 *lncTAM34a* over-expressing cell line showed a  
320 significant decrease of *CCND1* levels compared to the mock control.  
321 Collectively, these results indicate that *lncTAM34a*-mediated induction of  
322 *miR34a* is sufficient to result in the corresponding *miR34a*-directed effects on  
323 cell cycle.

324

325 *miR34a* is also a well-known inhibitor of cellular growth via its ability to  
326 negatively regulate growth factor signaling. Furthermore, starvation has been  
327 shown to induce *miR34a* expression causing down-regulation of numerous  
328 pro-survival growth factors (Lal et al. 2011). We further interrogated the  
329 effects of *lncTAM34a* over-expression by monitoring the growth of the PC3  
330 stable cell lines in both normal and starvation conditions via confluency  
331 measurements over a 35-hour period. Under normal growth conditions there  
332 is a small but significant reduction ( $P = 3.0\text{e-}8$ ; linear regression, **Fig. 3c**) in  
333 confluency in the *lncTAM34a* over-expressing cell lines compared to mock  
334 control. However, these effects on cell growth are drastically increased in

335 starvation conditions ( $P = 9.5e-67$ ; linear regression; **Fig. 3c**). This is in  
336 agreement with our previous results, and suggests that *lncTAM34a*-mediated  
337 increases in *miR34a* expression are crucial under conditions of stress and  
338 necessary for the initiation of an appropriate cellular response. In summary,  
339 we find that over-expression of *lncTAM34a* is sufficient to  
340 increase *miR34a* expression and gives rise to known phenotypes observed  
341 upon induction of *miR34a*.

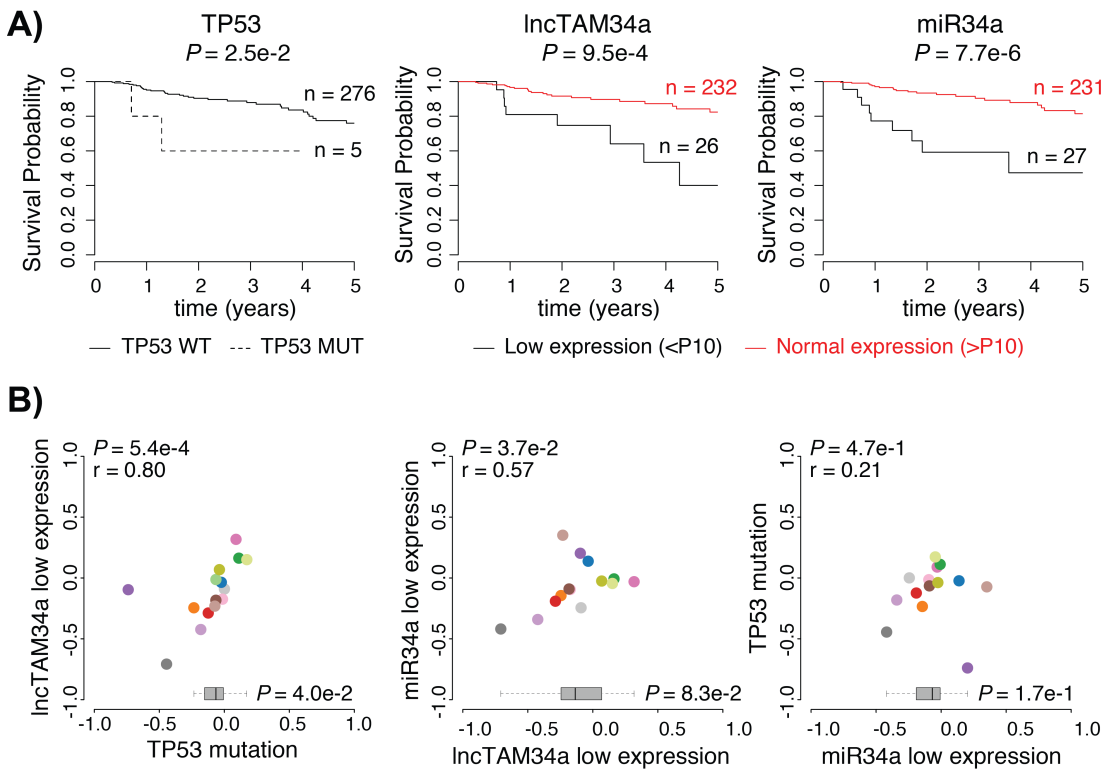
342

343 ***lncTAM34a* transcriptionally activates miR34a host gene**

344 Antisense RNAs have been reported to mediate their effects both via  
345 transcriptional and post-transcriptional mechanisms. Due to the fact that  
346 *miR34a* expression is undetected in wild type PC3 cells (**Fig. 1b**) but, upon  
347 over-expression of *lncTAM34a*, increases to detectable levels, we  
348 hypothesized that *lncTAM34a* is capable of regulating *miR34a* expression via  
349 a transcriptional mechanism. To ascertain if this is actually the case, we  
350 performed chromatin immunoprecipitation (ChIP) for phosphorylated  
351 polymerase II (polII) at the *miR34a* HG promoter in both *lncTAM34a* over-  
352 expressing and mock control cell lines. Our results indicated a clear increase  
353 in phosphorylated polII binding at the *miR34a* promoter upon *lncTAM34a*  
354 over-expression indicating the ability of *lncTAM34a* to regulate *miR34a* levels  
355 on a transcriptional level (**Fig. 3d**).

356

357

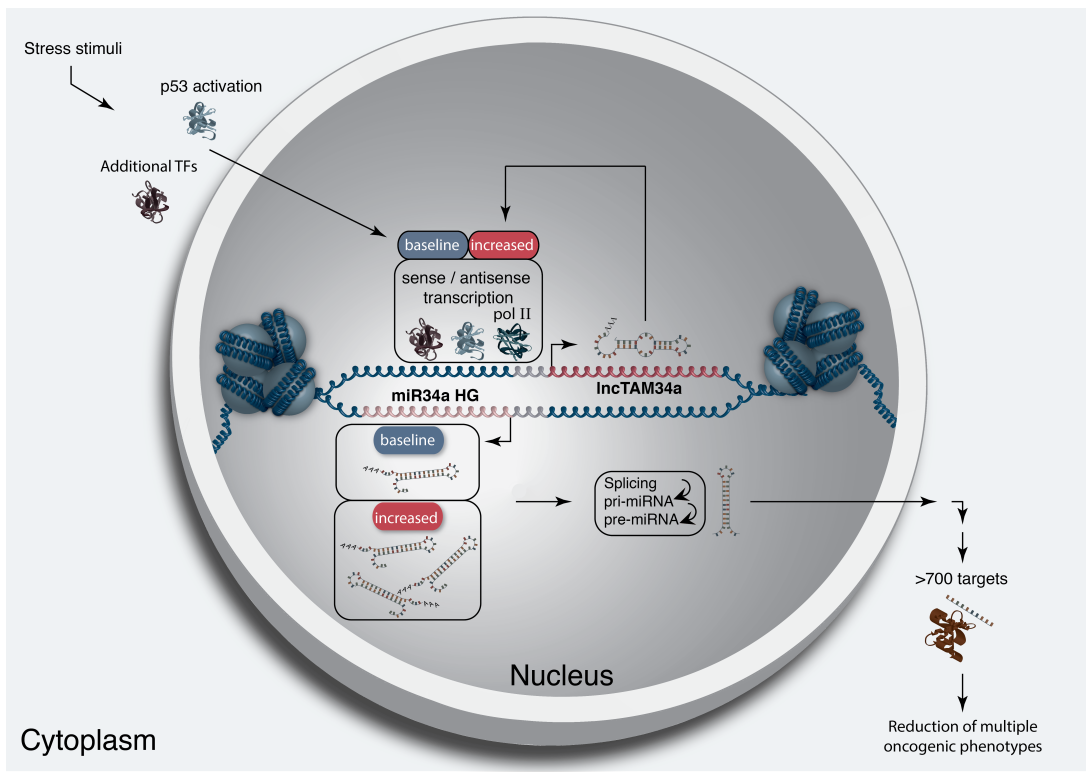


358

359 **Figure 4: Survival analysis in TCGA cancers.** A) Kaplan-Meier survival curves comparing the  
 360 effects of *TP53*-mutated samples (left), low *lncTAM34a* expression (middle) and low *miR34a*  
 361 expression (right) to control samples in papillary kidney cancer (results for other cancers in Figure 4-  
 362 Supplement 1). B) Correlation analysis between the effects on the 5-year survival probability of *TP53*-  
 363 mutated samples, low *lncTAM34a* expression, and low *miR34a* expression as indicated. For each  
 364 variable the 5-year survival probability was compared to the control group (negative value indicates  
 365 lower survival, positive value indicates higher survival). Spearman correlation coefficients are given on  
 366 top left of each plot. Each dot indicates one cancer type (see Fig. 1c for legend). Boxplots on the bottom  
 367 summarize the effects for the parameter on the x-axis, with indication of *P* values, as calculated using  
 368 paired Wilcoxon signed rank test. Low expression was defined as *TP53* non-mutated samples having  
 expression values in the bottom 10th percentile.

369  
370 **Low *lncTAM34a* expression levels are associated with decreased**  
371 **survival**

372  
373 As *TP53* mutations and low expression of *miR34a* have been associated with  
374 worse prognosis in cancer, we compared survival rates of samples with low  
375 expression of *lncTAM34a* (bottom 10th percentile) to control samples in 17  
376 cancer types from TCGA (**Figure 4-Supplement 1**) (Gallardo et al. 2009,  
377 Zenz et al. 2009, Liu et al. 2011). To correct for the effect of *TP53* mutations  
378 we focused on non-*TP53* mutated samples, and noted a worse survival for the  
379 low expression group in several cancers. This effect was most pronounced in  
380 papillary kidney cancer (unadjusted  $P=0.00095$ ; **Fig. 4a**). By systematically  
381 comparing 5-year survival probabilities between the low expression group and  
382 the control group for each cancer we found a median reduction of 5-year  
383 survival probability of 9.6% ( $P=0.083$ ; Wilcoxon signed rank test; **Fig. 4b**).  
384 Furthermore, we found that *lncTAM34a* expression showed similar patterns in  
385 terms of direction and strength of association with 5-year survival probability  
386 as *miR34a* expression ( $r=0.57$ ,  $P=0.037$ ) and *TP53* mutations ( $r=0.80$ ,  
387  $P=0.00054$ ) across the different cancer types (**Fig. 4b**). Although these results  
388 do not implicate any causal relationship, they do indicate a striking similarity  
389 between the association of worse prognosis and *TP53* mutations, low  
390 *miR34a*, and low *lncTAM34a* expression.



391

392 **Figure 5: A graphical summary of the proposed *IncTAM34a* function.** Stress stimuli, originating in  
 393 the cytoplasm or nucleus, activate TP53 as well as additional factors. These factors then bind to  
 394 the *miR34a* promoter and drive baseline transcription levels of the sense and antisense  
 395 strands. *IncTAM34a* serves to further increase *miR34a* HG transcription levels resulting in enrichment  
 396 of polymerase II at the *miR34a* promoter and a positive feed-forward loop. *miR34a* HG then, in turn,  
 397 is spliced and processed in multiple steps before the mature *miR34a* binds to the RISC complex allowing  
 398 it to repress its targets and exert its tumor suppressive effects.

399 **Discussion**

400  
401 Multiple studies have previously shown asRNAs to be crucial for the  
402 appropriate regulation of cancer-associated protein-coding genes and that  
403 their dysregulation can lead to perturbation of tumor suppressive and  
404 oncogenic pathways, as well as, cancer-related phenotypes (Yu et al. 2008,  
405 Yap et al. 2010, Serviss et al. 2014, Balbin et al. 2015). Here we show that  
406 asRNAs are also capable of regulating cancer-associated miRNAs resulting in  
407 similar consequences as protein-coding gene dysregulation (**Fig. 4**).  
408 Interestingly, we show that, both in the presence and absence of  
409 *TP53*, *lncTAM34a* provides an additional regulatory level to control *miR34a*  
410 expression in both homeostasis and upon encountering various forms of  
411 cellular stress. Furthermore, we find that *lncTAM34a*-mediated increase in  
412 *miR34a* expression is sufficient to drive the appropriate cellular responses to  
413 these stress stimuli (**Fig. 2d and Fig. 3c**). Previous studies have exploited  
414 various molecular biology methods to up-regulate *miR34a* expression in a  
415 *TP53*-deficient background showing similar phenotypic outcomes although,  
416 here we show a novel mechanism by which this can be achieved in an  
417 endogenous manner (Liu et al. 2011, Ahn et al. 2012, Yang et al. 2012,  
418 Stahlhut et al. 2015, Wang et al. 2015).

419

420 In agreement with previous studies, we demonstrate that upon encountering  
421 various types of cellular stress, *TP53* in concert with additional factors initiate  
422 transcription at the *miR34a* locus, thus increasing the levels of *lncTAM34a*  
423 and *miR34a* (Rashi-Elkeles et al. 2014, Hunten et al. 2015, Leveille et al.  
424 2015, Ashouri et al. 2016, Kim et al. 2017). We found that overexpression of

425 *IncTAM34a* leads to recruitment of polII to the *miR34a* promoter and  
426 hypothesize that *IncTAM34a* may provide positive feedback for *miR34a*  
427 expression whereby it serves as a scaffold for the recruitment of additional  
428 factors that facilitate polII-mediated transcription. In this manner, *miR34a*  
429 expression is induced, driving a shift towards a reduction in growth factor  
430 signaling, senescence, and in some cases apoptosis. On the other hand, in  
431 cells without functional TP53, other factors, which typically act independently  
432 or in concert with TP53, may initiate transcription of the *miR34a* locus. Due to  
433 the fact that *IncTAM34a* can alter miR34a expression in these cells, we  
434 suggest that it is interacting with one of these additional factors, possibly  
435 recruiting it to the *miR34a* locus in order to drive *miR34a* transcription, similar  
436 to mechanisms described for other lncRNAs (Hung et al. 2011, Ng et al. 2012,  
437 Ng et al. 2013). The head-to-head orientation of the *miR34a* HG and  
438 *IncTAM34a* causes sequence complementarity between the RNA and the  
439 promoter DNA, making targeting by direct binding an attractive mechanism.  
440 Previous reports have also illustrated the ability of asRNAs to form hybrid  
441 DNA:RNA R-loops and, thus, facilitate an open chromatin structure and the  
442 transcription of the sense gene (Boque-Sastre et al. 2015). The fact that the  
443 p1 construct only contains a small portion (307 bp) of the *IncTAM34a*  
444 transcript indicates that this portion is sufficient to give rise to at least a partial  
445 *miR34a* inducing response and therefore, that *IncTAM34a* may be able to  
446 facilitate *miR34a* expression independent of additional factors (**Fig 2d, Figure**  
447 **2-Figure Supplement 2a**). Nevertheless, further work will need to be  
448 performed to explore the mechanism whereby *IncTAM34a* regulates *miR34a*  
449 gene expression.

450

451 An antisense transcript arising from the *miR34a* locus, *Lnc34a*, has been  
452 previously reported to negatively regulate the expression of *miR34a* (Wang et  
453 al. 2016). Although the *Lnc34a* and *IncTAM34a* transcripts share some  
454 sequence similarity, we believe them to be separate RNAs that are,  
455 potentially, different isoforms of the same gene. We utilized CAGE and  
456 RNAseq data from the ENCODE project to evaluate the presence of  
457 *IncTAM34a* and *Lnc34a* in 28 and 36 commonly used cancer cell lines,  
458 respectively. Although the results show the presence of *IncTAM34a* in these  
459 cell lines, we find no evidence for *Lnc34a* transcription (**Supplementary**  
460 **Document 1**). These results are in line with the findings of Wang et al.  
461 indicating that *Lnc34a* is highly expressed in colon cancer stem cell spheres  
462 compared to all other cell types used in their study and may not be broadly  
463 expressed in other tissues or tumor types. The fact that *IncTAM34a* and  
464 *Lnc34a* would appear to have opposing roles in their regulation of *miR34a*,  
465 further underlines the complexity of the regulation at this locus.

466

467 Clinical trials utilizing *miR34a* replacement therapy have previously been  
468 conducted but, disappointingly, were terminated after adverse side effects of  
469 an immunological nature were observed in several of the patients (Slabakova  
470 et al. 2017). Although it is not presently clear if these side effects were caused  
471 by *miR34a* or the liposomal carrier used to deliver the miRNA, the multitude of  
472 evidence indicating *miR34a*'s crucial role in oncogenesis still makes its  
473 therapeutic induction an interesting strategy and needs further investigation.  
474 Our results indicate an association between survival probability and low

475 *lncTAM34a* expression making it an attractive candidate for controlled  
476 preclinical studies. Due to *lncTAM34a*-mediated positive feedback on *miR34a*  
477 expression, initiation of this feedback mechanism may provide a sustained  
478 *miR34a* induction in a relatively more robust manner than *miR34a*  
479 replacement alone. In summary, our results have identified *lncTAM34a* as a  
480 vital component in the regulation of *miR34a* and its particular importance in  
481 typical examples of cellular stress encountered in cancer. On a broader level,  
482 the conclusions drawn in this study provide an example of asRNA-mediated  
483 regulation of a clinically relevant cancer-associated miRNA and contribute to  
484 fundamental knowledge concerning *miR34a* regulation.

485

## 486 Materials and Methods

### 487 Cell Culture

488 All cell lines were cultured at 5% CO<sub>2</sub> and 37°C with HEK293T, Saos2, and  
489 Skov3 cells cultured in DMEM high glucose (GE Healthcare Life Sciences,  
490 Hyclone, Amersham. UK, Cat# SH30081), HCT116 and U2OS cells in  
491 McCoy's 5a (ThermoFisher Scientific, Pittsburgh, MA, USA. Cat# SH30200),  
492 and PC3 cells in RPMI (GE Healthcare Life Sciences, Hyclone, Cat#  
493 SH3009602) and 2 mM L-glutamine (GE Healthcare Life Sciences, Hyclone,  
494 Cat# SH3003402). All growth mediums were supplemented with 10% heat-  
495 inactivated FBS (ThermoFisher Scientific, Gibco, Cat# 12657029) and 50  
496 µg/ml of streptomycin (ThermoFisher Scientific, Gibco, Cat# 15140122) and  
497 50 µg/ml of penicillin (ThermoFisher Scientific, Gibco, Cat# 15140122). All cell  
498 lines were purchased from ATCC, tested negative for mycoplasma, and their  
499 identity was verified via STR profiling.

500  
501 **Bioinformatics, Data Availability, and Statistical Testing**

502 The USCS genome browser (Kent et al. 2002) was utilized for the  
503 bioinformatic evaluation of antisense transcription utilizing the RefSeq  
504 (O'Leary et al. 2016) gene annotation track.

505

506 All raw experimental data, code used for analysis, and supplementary  
507 methods are available for review at (Serviss 2017) and are provided as an R  
508 package. All analysis took place using the R statistical programming language  
509 (Team 2017) using external packages that are documented in the package  
510 associated with this article (Wilkins , Chang 2014, Wickham 2014, Therneau  
511 2015, Wickham 2016, Allaire et al. 2017, Arnold 2017, Wickham 2017,  
512 Wickham 2017, Wickham 2017, Xiao 2017, Xie 2017). The package facilitates  
513 replication of the operating system and package versions used for the original  
514 analysis, reproduction of each individual figure and figure supplement  
515 included in the article, and easy review of the code used for all steps of the  
516 analysis, from raw-data to figure.

517

518 The significance threshold (alpha) in this study was set to 0.05. Statistical  
519 testing was performed using an unpaired two sample Student's t-test unless  
520 otherwise specified.

521

522 **Coding Potential**

523 Protein-coding capacity was evaluated using the Coding-potential  
524 Assessment Tool (Wang et al. 2013) and Coding-potential Calculator (Kong et  
525 al. 2007) with default settings. Transcript sequences for use with Coding-

526 potential Assessment Tool were downloaded from the UCSC genome  
527 browser using the Ensembl  
528 accessions: *HOTAIR* (ENST00000455246), *XIST* (ENST00000429829), β-  
529 actin (ENST00000331789), Tubulin (ENST00000427480),  
530 and *MYC* (ENST00000377970). Transcript sequences for use with Coding-  
531 potential Calculator were downloaded from the UCSC genome browser using  
532 the following IDs: *HOTAIR* (uc031qho.1), β-actin (uc003soq.4).

533

#### 534 **Peptide identification in MS/MS spectra**

535 Orbitrap raw MS/MS files for 11 human cell lines were downloaded from the  
536 PRIDE repository (PXD002395; (Geiger et al. 2012)) converted to mzML  
537 format using msConvert from the ProteoWizard tool suite (Holman et al.  
538 2014). Spectra were then searched using MSGF+ (v10072) (Kim et al. 2014)  
539 and Percolator (v2.08) (Granholm et al. 2014). All searches were done  
540 against the human protein subset of Ensembl 75 in the Galaxy platform  
541 (Boekel et al. 2015) supplemented with the 6 frame translation of both the  
542 annotated (LOC102724571; hg38) and PCR cloned sequence of *IncTAM34a*  
543 (supplementary data; (Serviss 2017)). MSGF+ settings included precursor  
544 mass tolerance of 10 ppm, fully-tryptic peptides, maximum peptide length of  
545 50 amino acids and a maximum charge of 6. Fixed modification was  
546 carbamidomethylation on cysteine residues; a variable modification was used  
547 for oxidation on methionine residues. Peptide Spectral Matches found at 1%  
548 FDR (false discovery rate) were used to infer peptide identities. The output  
549 from all searches are available in (Serviss 2017).

550

551 **shRNAs**

552 shRNA-expressing constructs were cloned into the U6M2 construct using the  
553 BgIII and KpnI restriction sites as previously described (Amarzguioui et al.  
554 2005). shRNA constructs were transfected using Lipofectamine 2000 or 3000  
555 (ThermoFisher Scientific, Cat# 12566014 and L3000015). The sequences  
556 targeting renilla is as follows: shRenilla 1.1 (AAT ACA CCG CGC TAC TGG  
557 C), shRenilla 2.1 (TAA CGG GAT TTC ACG AGG C).

558

559 **Bi-directional Promoter Cloning**

560 The overlapping region (p1) corresponds with the sequence previously  
561 published as the TP53 binding site in (Raver-Shapira et al. 2007) which we  
562 synthesized, cloned into the pLucRluc construct (Polson et al. 2011), and  
563 sequenced to verify its identity.

564

565 **Promoter Activity**

566 Cells were co-transfected with the p1 renilla/firefly bidirectional promoter  
567 construct (Polson et al. 2011) and GFP by using Lipofectamine 2000 (Life  
568 Technologies, Cat# 12566014). The expression of GFP and luminescence  
569 was measured 24 h post transfection by using the Dual-Glo Luciferase Assay  
570 System (Promega, Cat# E2920) and detected by the GloMax-Multi+ Detection  
571 System (Promega, Cat# SA3030). The expression of luminescence was  
572 normalized to GFP.

573

574 **Generation of U6-expressed *IncTAM34a* Lentiviral Constructs**

575 The U6 promoter was amplified from the U6M2 cloning plasmid (Amarzguioui

576 et al. 2005) and ligated into the Not1 restriction site of the pHIV7-IMPDH2  
577 vector (Turner et al. 2012). *IncTAM34a* was PCR amplified and subsequently  
578 cloned into the Nhe1 and Pac1 restriction sites in the pHIV7-IMPDH2-U6  
579 plasmid.

580

581 **Lentiviral Particle production, infection, and selection**

582 Lentivirus production was performed as previously described in (Turner et al.  
583 2012). Briefly, HEK293T cells were transfected with viral and expression  
584 constructs using Lipofectamine 2000 (ThermoFisher Scientific, Cat#  
585 12566014), after which viral supernatants were harvested 48 and 72 hours  
586 post-transfection. Viral particles were concentrated using PEG-IT solution  
587 (Systems Biosciences, Palo Alto, CA, USA. Cat# LV825A-1) according to the  
588 manufacturer's recommendations. HEK293T cells were used for virus titration  
589 and GFP expression was evaluated 72hrs post-infection via flow cytometry  
590 (LSRII, BD Biosciences, San Jose, CA, USA) after which TU/ml was  
591 calculated.

592

593 Stable lines were generated by infecting cells with a multiplicity of infection of  
594 1 and subsequently initiating 1-2 µM mycophenolic acid-based (Merck,  
595 Kenilworth, NJ, USA. Cat# M5255) selection 48-72 hours post-infection. Cells  
596 were expanded as the selection process was monitored via flow cytometry  
597 analysis (LSRII, BD Biosciences) of GFP and selection was terminated once  
598 > 90% of the cells were GFP positive. Quantification of *IncTAM34a* over-  
599 expression and *miR34a* was performed in biological quintuplet for all cell  
600 lines.

601

602 **Western Blotting**

603 Samples were lysed in 50 mM Tris-HCl (Sigma Aldrich, St. Louis, MO, USA).  
604 Cat# T2663), pH 7.4, 1% NP-40 (Sigma Aldrich, Cat# I8896), 150 mM NaCl  
605 (Sigma Aldrich, Cat# S5886), 1 mM EDTA (Promega, Madison, WI, USA).  
606 Cat# V4231), 1% glycerol (Sigma Aldrich, Cat# G5516), 100 µM vanadate  
607 (Sigma Aldrich, Cat# S6508), protease inhibitor cocktail (Roche Diagnostics,  
608 Basel, Switzerland, Cat# 004693159001) and PhosSTOP (Roche  
609 Diagnostics, Cat# 04906837001). Lysates were subjected to SDS-PAGE and  
610 transferred to PVDF membranes. The proteins were detected by western blot  
611 analysis by using an enhanced chemiluminescence system (Western  
612 Lightning–ECL, PerkinElmer, Waltham, MA, USA. Cat# NEL103001EA).  
613 Antibodies used were specific for CCND1 1:1000 (Cell Signaling, Danvers,  
614 MA, USA. Cat# 2926), and GAPDH 1:5000 (Abcam, Cambridge, UK, Cat#  
615 ab9485). All western blot quantifications were performed using ImageJ  
616 (Schneider et al. 2012).

617

618 **RNA Extraction and cDNA Synthesis**

619 For downstream SYBR green applications, RNA was extracted using the  
620 RNeasy mini kit (Qiagen, Venlo, Netherlands, Cat# 74106) and subsequently  
621 treated with DNase (Ambion Turbo DNA-free, ThermoFisher Scientific, Cat#  
622 AM1907). 500ng RNA was used for cDNA synthesis using MuMLV  
623 (ThermoFisher Scientific, Cat# 28025013) and a 1:1 mix of oligo(dT) and  
624 random nanomers.

625

626 For analysis of miRNA expression with Taqman, samples were isolated with  
627 TRIzol reagent (ThermoFisher Scientific, Cat# 15596018) and further  
628 processed with the miRNeasy kit (Qiagen, Cat# 74106). cDNA synthesis was  
629 performed using the TaqMan MicroRNA Reverse Transcription Kit  
630 (ThermoFisher Scientific, Cat# 4366597) using the corresponding oligos  
631 according to the manufacturer's recommendations.

632

### 633 **QPCR and PCR**

634 PCR was performed using the KAPA2G Fast HotStart ReadyMix PCR Kit  
635 (Kapa Biosystems, Wilmington, MA, USA, Cat# KK5601) with corresponding  
636 primers. QPCR was carried out using KAPA 2G SYBRGreen (Kapa  
637 Biosystems, Cat# KK4602) using the Applied Biosystems 7900HT machine  
638 with the cycling conditions: 95 °C for 3 min, 95 °C for 3 s, 60 °C for 30 s.

639

640 QPCR for miRNA expression analysis was performed according to the primer  
641 probe set manufacturers recommendations (ThermoFisher Scientific) and  
642 using the TaqMan Universal PCR Master Mix (ThermoFisher Scientific, Cat#  
643 4304437) with the same cycling scheme as above. Primer and probe sets for  
644 TaqMan were also purchased from ThermoFisher Scientific (Life  
645 Technologies at time of purchase, TaqMan® MicroRNA Assay, hsa-miR-34a,  
646 human, Cat# 4440887, Assay ID: 000426 and Control miRNA Assay, RNU48,  
647 human, Cat# 4440887, Assay ID: 001006).

648

649 The ΔΔCt method was used to quantify gene expression. All QPCR-based  
650 experiments were performed in at least technical duplicate. Primers for all

651 PCR-based experiments are listed in **Supplementary Document 2** and  
652 arranged by figure.

653

654 **Cell Cycle Distribution**

655 Cells were washed in PBS and fixed in 4% paraformaldehyde at room  
656 temperature overnight. Paraformaldehyde was removed, and cells were re-  
657 suspended in 95% EtOH. The samples were then rehydrated in distilled  
658 water, stained with DAPI and analyzed by flow cytometry on a LSRII (BD  
659 Biosciences) machine. Resulting cell cycle phases were quantified using the  
660 ModFit software (Verity Software House, Topsham, ME, USA). Experiments  
661 were performed in biological quadruplet (PC3) or triplicate (Skov3). The log2  
662 fraction of cell cycle phase was calculated for each replicate and a two  
663 sample t-test was utilized for statistical testing.

664

665 **3' Rapid Amplification of cDNA Ends**

666 3'-RACE was performed as described as previously in (Johnsson et al. 2013).  
667 Briefly, U2OS cell RNA was polyA-tailed using yeast polyA polymerase  
668 (ThermoFisher Scientific, Cat# 74225Z25KU) after which cDNA was  
669 synthesized using oligo(dT) primers. Nested-PCR was performed first using a  
670 forward primer in *lncTAM34a* exon 1 and a tailed oligo(dT) primer followed by  
671 a second PCR using an alternate *lncTAM34a* exon 1 primer and a reverse  
672 primer binding to the tail of the previously used oligo(dT) primer. PCR  
673 products were gel purified and cloned the Strata Clone Kit (Agilent  
674 Technologies, Santa Clara, CA, USA. Cat# 240205), and sequenced.

675

676 **Chromatin Immunoprecipitation**

677 The ChIP was performed as previously described in (Johnsson et al. 2013)  
678 with the following modifications. Cells were crosslinked in 1% formaldehyde  
679 (Merck, Cat# 1040039025), quenched with 0.125M glycine (Sigma Aldrich,  
680 Cat# G7126), and lysed in cell lysis buffer comprised of: 5mM PIPES (Sigma  
681 Aldrich, Cat# 80635), 85mM KCL (Merck, Cat# 4936), 0.5% NP40 (Sigma  
682 Aldrich, Cat# I8896), protease inhibitor (Roche Diagnostics, Cat#  
683 004693159001). Samples were then sonicated in 50mM TRIS-HCL pH 8.0  
684 (Sigma Aldrich, MO, USA, Cat# T2663) 10mM EDTA (Promega, WI, USA,  
685 Cat# V4231), 1% SDS (ThermoFisher Scientific, Cat# AM9822), and protease  
686 inhibitor (Roche Diagnostics, Cat# 004693159001) using a Bioruptor  
687 Sonicator (Diagenode, Denville, NJ, USA). Samples were incubated over  
688 night at 4°C with the polII antibody (Abcam, Cat# ab5095) and subsequently  
689 pulled down with Salmon Sperm DNA/Protein A Agarose (Millipore, Cat# 16-  
690 157) beads. DNA was eluted in an elution buffer of 1% SDS (ThermoFisher  
691 Scientific, Cat# AM9822) 100mM NaHCO3 (Sigma Aldrich, Cat# 71631),  
692 followed by reverse crosslinking, RNaseA (ThermoFisher Scientific, Cat#  
693 1692412) and protease K (New England Biolabs, Ipswich, MA, USA, Cat#  
694 P8107S) treatment. The DNA was eluted using Qiagen PCR purification kit  
695 (Cat# 28106) and quantified via QPCR. QPCR was performed in technical  
696 duplicate using the standard curve method and reported absolute values. The  
697 fraction of input was subsequently calculated using the mean of the technical  
698 replicates followed by calculating the fold over the control condition. Statistical  
699 testing was performed using 4 biological replicates with the null hypothesis  
700 that the true log2 fold change values were equal to zero.

701

702 **Confluency Analysis**

703 Cells were incubated in the Spark Multimode Microplate (Tecan, Männedorf,  
704 Switzerland) reader for 48 hours at 37°C with 5% CO<sub>2</sub> in a humidity chamber.  
705 Confluency was measured every hour using bright-field microscopy and the  
706 percentage of confluency was reported via the plate reader's inbuilt algorithm.  
707 Percentage of confluency was normalized to the control sample in each  
708 condition (shown in figure) and then ranked to move the data to a linear scale.  
709 Using the mean of the technical duplicates in three biological replicates, the  
710 rank was then used to construct a linear model, of the dependency of the rank  
711 on the time and cell lines variables for each growth condition. Reported *P*  
712 values are derived from the t-test, testing the null hypothesis that the  
713 coefficient estimate of the cell line variable is equal to 0.

714

715 **Pharmacological Compounds**

716 Doxorubicin was purchased from Teva (Petah Tikva, Israel, cat. nr. 021361).

717

718 **Cellular Localization Analysis**

719 Quantified RNAseq data from 11 cell lines from the GRCh38 assembly was  
720 downloaded from the ENCODE project database and quantifications for  
721 *IncTAM34a* (ENSG00000234546), GAPDH (ENSG00000111640), and  
722 MALAT1 (ENSG00000251562) were extracted. Cell lines for which data was  
723 downloaded include: A549, GM12878, HeLa-S3, HepG2, HT1080, K562  
724 MCF-7, NCI-H460, SK-MEL-5, SK-N-DZ, SK-N-SH. Initial exploratory analysis  
725 revealed that several cell lines should be removed from the analysis due to a)

726 a larger proportion of GAPDH in the nucleus than cytoplasm or b) variation of  
727 *lncTAM34a* expression is too large to draw conclusions, or c) they have no or  
728 low (<6 TPM) *lncTAM34a* expression. Furthermore, only polyadenylated  
729 libraries were used in the final analysis, due to the fact that the cellular  
730 compartment enrichment was improved in these samples. All analyzed genes  
731 are reported to be polyadenylated. In addition, only samples with 2 biological  
732 replicates were retained. For each cell type, gene, and biological replicate the  
733 fraction of transcripts per million (TPM) in each cellular compartment was  
734 calculated as the fraction of TPM in the specific compartment by the total  
735 TPM. The mean and standard deviation for the fraction was subsequently  
736 calculated for each cell type and cellular compartment and this information  
737 was represented in the final figure.

738

### 739 **CAGE Analysis**

740 All available CAGE data from the ENCODE project (Consortium 2012) for 36  
741 cell lines was downloaded from the UCSC genome browser (Kent et al. 2002)  
742 for genome version hg19. Of these, 28 cell lines had CAGE transcription start  
743 sites (TSS) mapping to the plus strand of chromosome 1 and in regions  
744 corresponding to 200 base pairs upstream of the *Lnc34a* start site (9241796 -  
745 200) and 200 base pairs upstream of the GENCODE annotated *lncTAM34a*  
746 start site (9242263 + 200). These cell lines included: HFDPC, H1-hESC,  
747 HMEpC, HAoEC, HPIEpC, HSaVEC, GM12878, hMSC-BM, HUVEC,  
748 AG04450, hMSC-UC, IMR90, NHDF, SK-N-SH\_RA, BJ, HOB, HPC-PL,  
749 HAoAF, NHEK, HVMF, HWP, MCF-7, HepG2, hMSC-AT, NHEM.f\_M2,  
750 SkMC, NHEM\_M2, and HCH. In total 74 samples were included. 17 samples

751 were polyA-, 47 samples were polyA+, and 10 samples were total RNA. In  
752 addition, 34 samples were whole cell, 15 enriched for the cytosolic fraction, 15  
753 enriched for the nucleolus, and 15 enriched for the nucleus. All CAGE  
754 transcription start sites were plotted and the RPKM of the individual reads was  
755 used to color each read to indicate their relative abundance. In cases where  
756 CAGE TSS spanned identical regions, the RPMKs of the regions were  
757 summed and represented as one CAGE TSS in the figure. In addition, a  
758 density plot shows the distribution of the CAGE reads in the specified  
759 interval.

760

## 761 **Splice Junction Analysis**

762 All available whole cell (i.e. non-fractionated) spliced read data originating  
763 from the Cold Spring Harbor Lab in the ENCODE project (Consortium 2012)  
764 for 38 cell lines was downloaded from the UCSC genome browser (Kent et al.  
765 2002). Of these cell lines, 36 had spliced reads mapping to the plus strand of  
766 chromosome 1 and in the region between the *Lnc34a* start (9241796) and  
767 transcription termination (9257102) site (note that *lncTAM34a* resides totally  
768 within this region). Splice junctions from the following cell lines were included  
769 in the final figure: A549, Ag04450, Bj, CD20, CD34 mobilized, Gm12878,  
770 H1hesc, Haoaf, Haoec, Hch, Helas3, Hepg2, Hfdpc, Hmec, Hmepc, Hmscat,  
771 Hmscbm, Hmscuc, Hob, Hpcpl, Hpiepc, Hsavec, Hsmmm, Huvec, Hvmaf, Hwp,  
772 Imr90, Mcf7, Monocd14, Nhdf, Nhek, Nhemfm2, Nhemm2, Nhlf, Skmc, and  
773 Sknsh. All splice junctions were included in the figure and colored according  
774 to the number of reads corresponding to each. In cases where identical reads  
775 were detected multiple times, the read count was summed and represented

776 as one read in the figure.

777

## 778 **TCGA Data Analysis**

779 RNA-Seq data and copy number data were downloaded from TCGA and  
780 processed as described previously (Ashouri et al. 2016). Briefly, RNA-Seq  
781 data were aligned to the human hg19 assembly and quantified using  
782 GENCODE (v19) annotated HTSeq-counts and FPKM normalizations.  
783 Expression data from *miR34a* and *lncTAM34a* (identified as RP3-510D11.2)  
784 were used for further analysis. Copy number amplitudes for GENCODE genes  
785 were determined from segmented copy-number data. Samples that were  
786 diploid for *lncTAM34a* were identified as those samples that had copy number  
787 amplitudes between -0.1 and 0.1.

788

789 Somatic mutation data were downloaded from the Genomics Data Commons  
790 data portal (GDC) as mutation annotation format (maf) files, called using  
791 Mutect2 on 30/10/2017 (v7) (Grossman et al. 2016).

792

793 Survival analysis was performed on TCGA vital state and follow-up data,  
794 downloaded from GDC on 27/10/2017 using the R survival package  
795 (Therneau 2015).

796

## 797 **Acknowledgments**

798 The authors would like to kindly thank Martin Enge for his critical review of the  
799 manuscript and fruitful discussions.

800

## 801 **Competing Interests**

802

803 The authors declare no competing interests.

804

805

806 **Funding**

807

808 This work has been supported by the Swedish Research Council [521-2012-  
809 2037], Swedish Cancer Society [150768], Cancer Research Foundations of  
810 Radiumhemmet [144063] and the Swedish Childhood Cancer Foundation  
811 [PR2015-0009].

812

813

814 **Figure Supplements**

815

816 Figure 1-Supplement 1: TCAG expression levels and correlation analysis  
817 statistics.

818

819 Figure 1-Supplement 2: Molecular characteristics of *lncTAM34a*.

820

821 Figure 2-Supplement 1: A schematic representation of the p1 construct.

822

823 Figure 2-Supplement 2: Evaluating the effects of *lncTAM34a* down-regulation.

824

825 Figure 3-Supplement 1: Physiological relevance of *lncTAM34a*  
826 overexpression.

827

828 Figure 3-Supplement 2: Effects of *lncTAM34a* overexpression on cyclin D1.

829

830 Figure 4-Supplement 1: Survival analysis in 17 cancers from TCGA.

831

832 Supplementary Document 1: Evaluating the relationship between *lncTAM34a*  
833 and *Lnc34a*.\*

834

835 Supplementary Document 2: A table of primers used in this study.\*

836

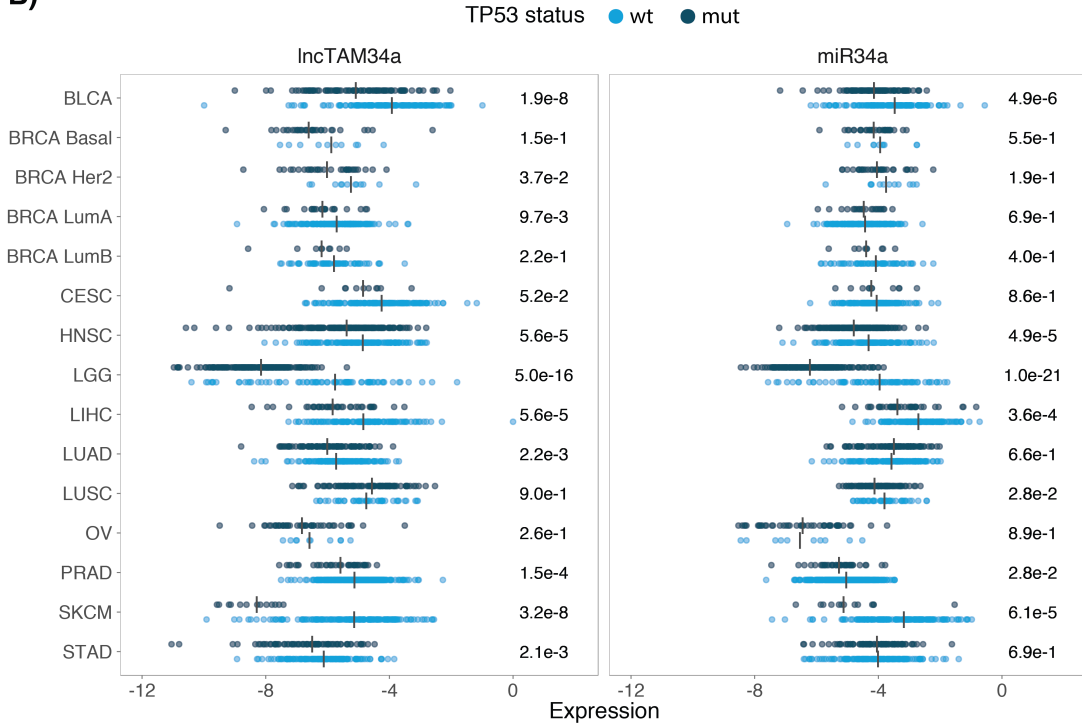
837 \*Please note that in the initial submission these documents are included after  
838 the References section of the pdf file.

839 **Supplementary Figures**

**A)**

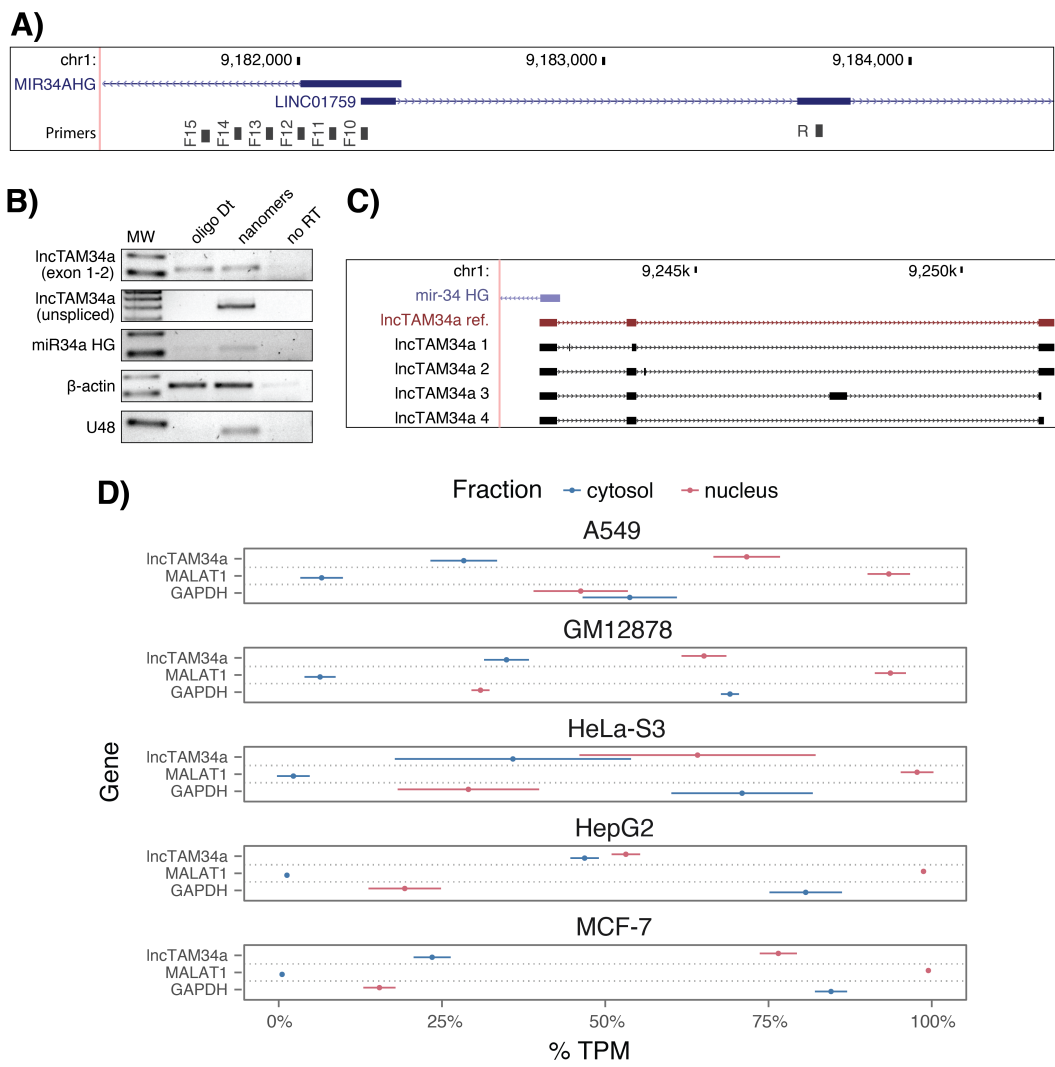
cancer	all n	all rho	all p	TP53wt n	TP53wt rho	TP53wt p	TP53mut n	TP53mut rho	TP53mut p
Adrenocortical carcinoma ( ACC )	10	0.55	1.04e-01	10	0.55	1.04e-01	NA	NA	NA
Bladder Urothelial Carcinoma ( BLCA )	228	0.51	7.89e-17	134	0.45	3.86e-08	94	0.43	1.73e-05
Breast invasive carcinoma ( BRCA ) Basal	42	0.57	9.54e-05	10	0.62	6.02e-02	32	0.57	7.41e-04
Breast invasive carcinoma ( BRCA ) Her2	44	0.15	3.39e-01	12	0.22	4.85e-01	32	0.07	7.10e-01
Breast invasive carcinoma ( BRCA ) LumA	199	0.34	8.22e-07	177	0.34	2.96e-06	22	0.49	2.31e-02
Breast invasive carcinoma ( BRCA ) LumB	70	0.17	1.57e-01	61	0.15	2.53e-01	9	0.17	6.78e-01
Cervical squamous cell carcinoma and endocervical adenocarcinoma ( CESC )	156	0.14	8.37e-02	145	0.16	5.45e-02	11	-0.05	9.03e-01
Head and Neck squamous cell carcinoma ( HNSC )	313	0.54	8.38e-25	123	0.61	0.00e+00	190	0.45	9.68e-11
Kidney Chromophobe ( KICH )	5	0.60	3.50e-01	5	0.60	3.50e-01	NA	NA	NA
Kidney renal clear cell carcinoma ( KIRC )	142	0.35	2.06e-05	141	0.34	4.41e-05	NA	NA	NA
Kidney renal papillary cell carcinoma ( KIRP )	167	0.45	9.16e-10	163	0.45	2.04e-09	4	0.80	3.33e-01
Brain Lower Grade Glioma ( LGG )	271	0.63	9.92e-32	76	0.73	0.00e+00	195	0.39	2.26e-08
Liver hepatocellular carcinoma ( LIHC )	153	0.56	3.64e-14	114	0.52	4.18e-09	39	0.45	3.95e-03
Lung adenocarcinoma ( LUAD )	234	0.28	1.15e-05	128	0.36	2.87e-05	106	0.23	1.91e-02
Lung squamous cell carcinoma ( LUSC )	139	0.23	6.74e-03	42	0.04	7.93e-01	97	0.33	9.91e-04
Ovarian serous cystadenocarcinoma ( OV )	56	0.23	8.37e-02	10	0.84	4.46e-03	46	0.15	3.31e-01
Prostate adenocarcinoma ( PRAD )	413	0.47	1.33e-23	375	0.46	6.13e-21	38	0.45	4.58e-03
Skin Cutaneous Melanoma ( SKCM )	165	0.65	5.43e-21	152	0.61	7.85e-17	13	0.43	1.40e-01
Stomach adenocarcinoma ( STAD )	225	0.37	8.23e-09	145	0.37	5.71e-06	80	0.42	1.03e-04
Thyroid carcinoma ( THCA )	469	0.46	1.07e-25	467	0.46	4.06e-26	NA	NA	NA

**B)**



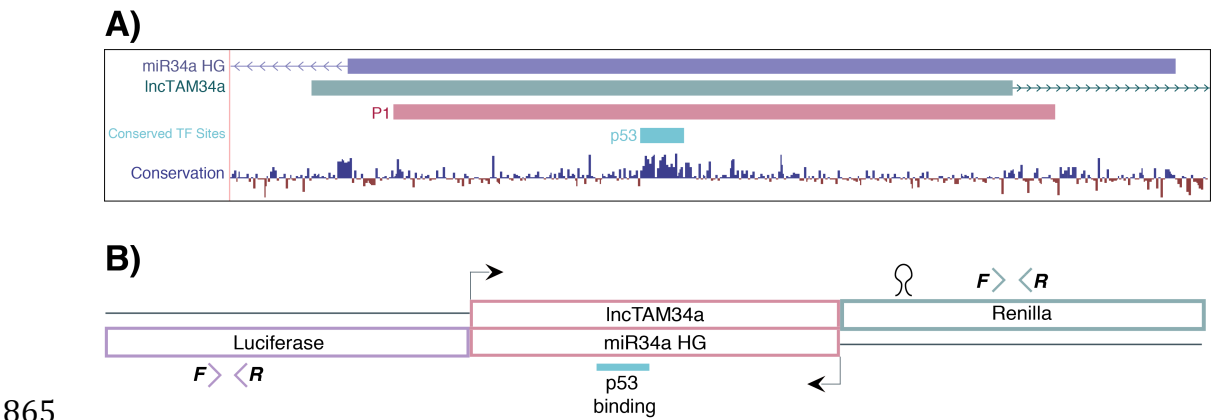
840  
841

842 **Figure 1 Supplement 1: TCGA normalized expression levels and correlation analysis statistics.**  
843 A) Spearman's rho and P values (p) from the correlation analysis in Figure 1a between *miR34a* and  
844 *lncTAM34a* expression in *TP53* wild type (wt) and mutated (mut) samples within TCGA cancer types.  
845 NA indicates not applicable, due to a lack of data for the specific group. B) Expression levels of  
846 *miR34a* and *lncTAM34a* in *TP53* wt and nonsynonymous mutation samples. Expression was quantified  
847 by the log2 ratio of expression of the gene to its maximal expression value. Vertical lines indicate the  
848 median. P values are indicated on the right side of each panel and are derived from comparing the  
849 *TP53* wild type samples to the samples with a nonsynonymous mutation using a two-sided Wilcoxon  
850 signed rank test. Only samples that had at least 5 samples per comparison were included. In addition,  
851 only samples that were diploid at the *miR34a* locus were used for the analysis to avoid copy number  
852 bias.

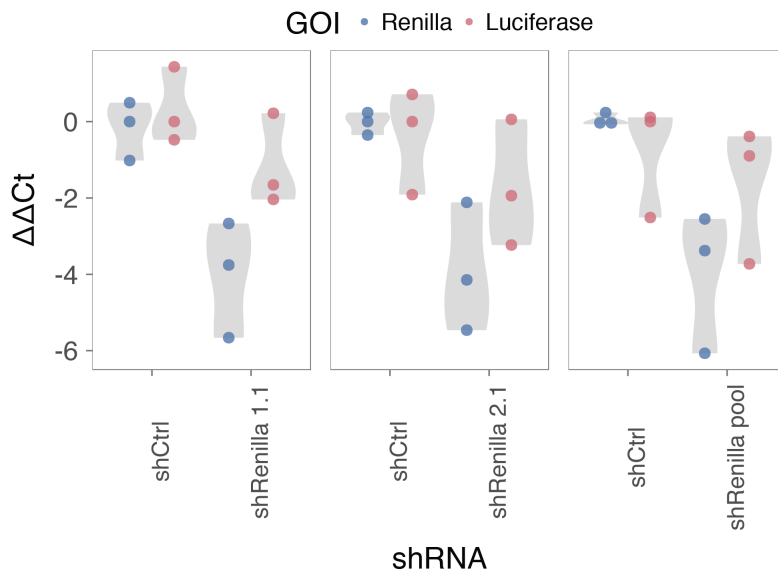


853  
854  
855  
856  
857  
858  
859  
860  
861  
862  
863  
864

**Figure 1 Supplement 2: Molecular characteristics of lncTAM34a.** **A)** A schematic representation of the primer placement in the primer walk assay. **B)** Polyadenylation status of spliced and unspliced lncTAM34a in HEK293T cells. **C)** Sequencing results from the analysis of lncTAM34a isoforms in U2OS cells. lncTAM34a ref. refers to the full-length transcript as defined by the 3'-RACE and primer walk assay. **D)** Analysis of coding potential of the lncTAM34a transcript using the Coding-potential Calculator. **E)** RNAseq data from five fractionated cell lines in the ENCODE project showing the percentage of transcripts per million (TPM) for lncTAM34a. MALAT1 (nuclear localization) and GAPDH (cytoplasmic localization) are included as fractionation controls. Points represent the mean and horizontal lines represent the standard deviation from two biological replicates.

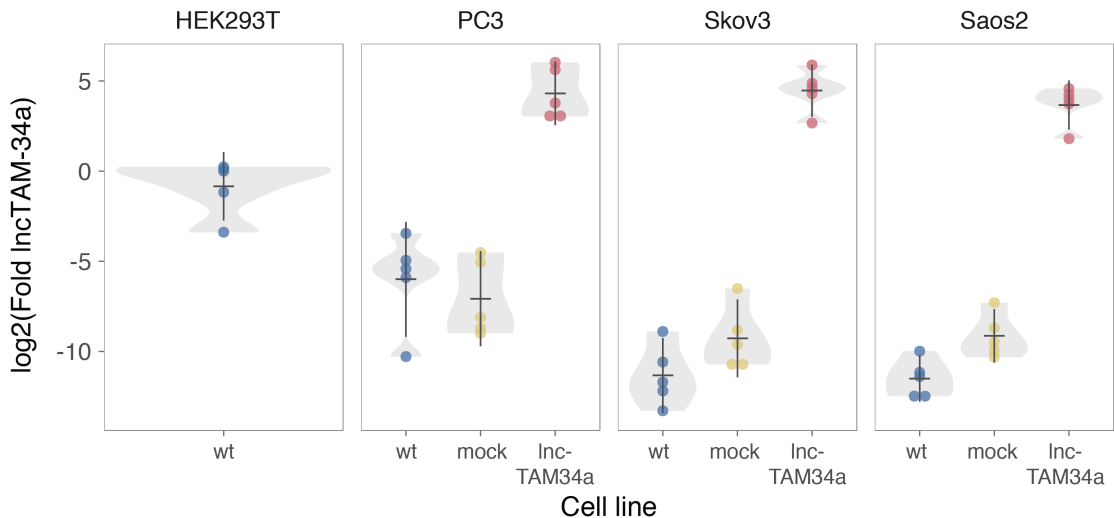


865  
866  
867 **Figure 2 Supplement 1: A schematic representation of the p1 construct.** **A)** A UCSC genome  
868 browser illustration indicating the location of the promoter region cloned into the p1 construct  
869 including the conserved TP53-binding site. **B)** A representative picture of the p1 construct including  
870 the forward (F) and reverse (R) primer locations and the renilla shRNA targeting site.



871  
872  
873  
874  
875  
876  
877

**Figure 2 Supplement 2: Evaluating the effects of *lncTAM34a* down-regulation.** HEK293T cells were co-transfected with the p1 construct and either shRenilla or shControl. Renilla and luciferase levels were measured with QPCR 48 hours after transfection. Individual points represent independent experiments with the gray shadow indicating the density of the points. The experiment was performed in biological triplicate.



878  
879

880 **Figure 3 Supplement 1: Physiological relevance of *lncTAM34a* overexpression.** Comparison  
881 of *lncTAM34a* expression in HEK293T cells (high endogenous *lncTAM34a*), and the wild-type (wt),  
882 mock, and *lncTAM34a* over-expressing stable cell lines.

883  
884  
885  
886  
887

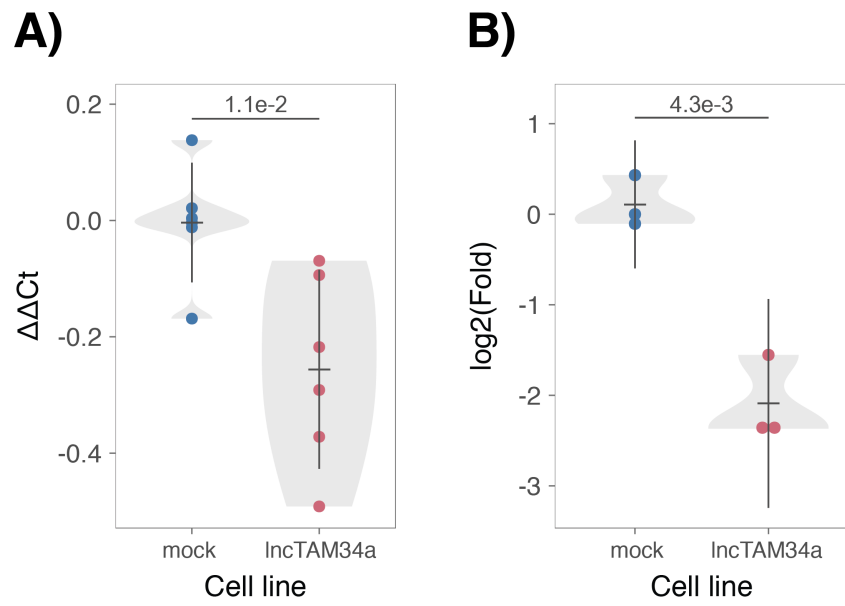
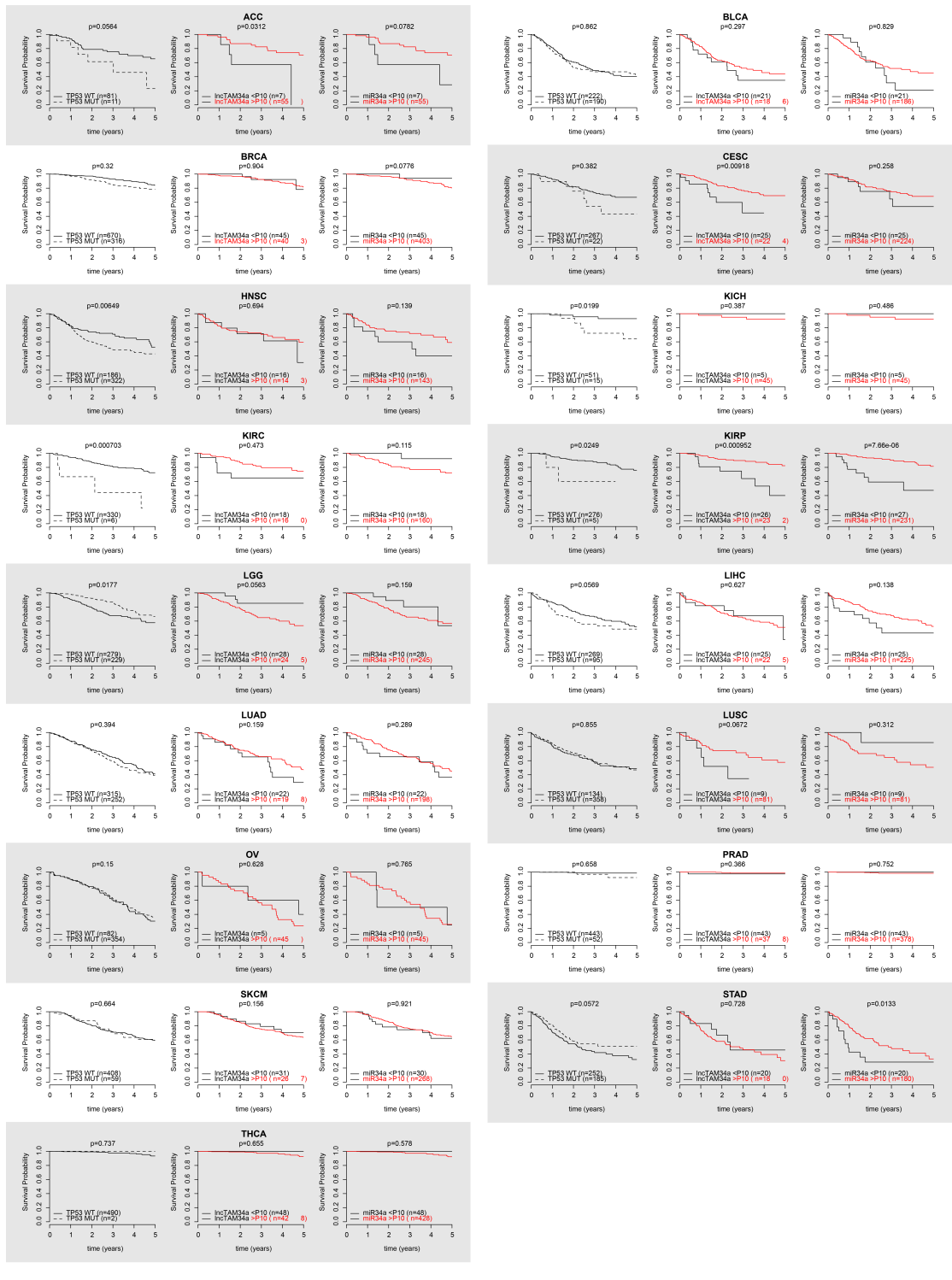


**Figure 3 Supplement 2:** Effects of *lncTAM34a* overexpression on cyclin D1. CCND1 expression (A) and western blot quantification of protein levels (B) in *lncTAM34a* over-expressing PC3 stable cell lines. Experiments were performed in biological sextuplets (A) or triplicates (B).



888

**Figure 4-Supplement 1: Survival analysis in 17 cancers from TCGA.** Kaplan-Meier survival curves comparing the survival of *TP53*-mutated samples (left), low *IncTAM34a* expression (middle) and low *miR34a* expression (right) to control samples in 17 cancer types from TCGA. Low expression was defined as *TP53* non-mutated samples having expression values in the bottom 10th percentile.

893

894

895 **References**

896

897 Agostini, M., P. Tucci, R. Killick, E. Candi, B. S. Sayan, P. Rivetti di Val Cervo, P.  
 898 Nicotera, F. McKeon, R. A. Knight, T. W. Mak and G. Melino (2011). "Neuronal  
 899 differentiation by TAp73 is mediated by microRNA-34a regulation of synaptic  
 900 protein targets." *Proc Natl Acad Sci U S A* **108**(52): 21093-21098. DOI:  
 901 10.1073/pnas.1112061109

902

903 Ahn, Y. H., D. L. Gibbons, D. Chakravarti, C. J. Creighton, Z. H. Rizvi, H. P. Adams, A.  
 904 Pertsemlidis, P. A. Gregory, J. A. Wright, G. J. Goodall, E. R. Flores and J. M. Kurie  
 905 (2012). "ZEB1 drives prometastatic actin cytoskeletal remodeling by  
 906 downregulating miR-34a expression." *J Clin Invest* **122**(9): 3170-3183. DOI:  
 907 10.1172/JCI63608

908

909 Allaire, J., Y. Xie, J. McPherson, J. Luraschi, K. Ushey, A. Atkins, H. Wickham, J.  
 910 Cheng and W. Chang (2017). rmarkdown: Dynamic Documents for R. R package  
 911 version 1.8. <https://CRAN.R-project.org/package=rmarkdown>

912

913 Amarzguioui, M., J. J. Rossi and D. Kim (2005). "Approaches for chemically  
 914 synthesized siRNA and vector-mediated RNAi." *FEBS Lett* **579**(26): 5974-5981.  
 915 DOI: 10.1016/j.febslet.2005.08.070

916

917 Arnold, J. B. (2017). ggthemes: Extra Themes, Scales and Geoms for 'ggplot2'. R  
 918 package version 3.4.0. <https://CRAN.R-project.org/package=ggthemes>

919

920 Ashouri, A., V. I. Sayin, J. Van den Eynden, S. X. Singh, T. Papagiannakopoulos and  
 921 E. Larsson (2016). "Pan-cancer transcriptomic analysis associates long non-  
 922 coding RNAs with key mutational driver events." *Nature Communications* **7**:  
 923 13197. DOI: 10.1038/ncomms13197

924

925 Balbin, O. A., R. Malik, S. M. Dhanasekaran, J. R. Prensner, X. Cao, Y. M. Wu, D.  
 926 Robinson, R. Wang, G. Chen, D. G. Beer, A. I. Nesvizhskii and A. M. Chinnaiyan  
 927 (2015). "The landscape of antisense gene expression in human cancers." *Genome  
 928 Res* **25**(7): 1068-1079. DOI: 10.1101/gr.180596.114

929

930 Boekel, J., J. M. Chilton, I. R. Cooke, P. L. Horvatovich, P. D. Jagtap, L. Kall, J. Lehtio,  
 931 P. Lukasse, P. D. Moerland and T. J. Griffin (2015). "Multi-omic data analysis using  
 932 Galaxy." *Nat Biotechnol* **33**(2): 137-139. DOI: 10.1038/nbt.3134

933

934 Boque-Sastre, R., M. Soler, C. Oliveira-Mateos, A. Portela, C. Moutinho, S. Sayols, A.  
 935 Villanueva, M. Esteller and S. Guil (2015). "Head-to-head antisense transcription  
 936 and R-loop formation promotes transcriptional activation." *Proc Natl Acad Sci U  
 937 S A* **112**(18): 5785-5790. DOI: 10.1073/pnas.1421197112

938

939 Chang, T. C., D. Yu, Y. S. Lee, E. A. Wentzel, D. E. Arking, K. M. West, C. V. Dang, A.  
 940 Thomas-Tikhonenko and J. T. Mendell (2008). "Widespread microRNA  
 941 repression by Myc contributes to tumorigenesis." *Nat Genet* **40**(1): 43-50. DOI:  
 942 10.1038/ng.2007.30

943  
944 Chang, W. (2014). extrafont: Tools for using fonts. R package version 0.17.  
945 <https://CRAN.R-project.org/package=extrafont>  
946  
947 Chen, J., M. Sun, W. J. Kent, X. Huang, H. Xie, W. Wang, G. Zhou, R. Z. Shi and J. D.  
948 Rowley (2004). "Over 20% of human transcripts might form sense-antisense  
949 pairs." *Nucleic Acids Res* **32**(16): 4812-4820. DOI: 10.1093/nar/gkh818  
950  
951 Cheng, J., L. Zhou, Q. F. Xie, H. Y. Xie, X. Y. Wei, F. Gao, C. Y. Xing, X. Xu, L. J. Li and S.  
952 S. Zheng (2010). "The impact of miR-34a on protein output in hepatocellular  
953 carcinoma HepG2 cells." *Proteomics* **10**(8): 1557-1572. DOI:  
954 10.1002/pmic.200900646  
955  
956 Chim, C. S., K. Y. Wong, Y. Qi, F. Loong, W. L. Lam, L. G. Wong, D. Y. Jin, J. F. Costello  
957 and R. Liang (2010). "Epigenetic inactivation of the miR-34a in hematological  
958 malignancies." *Carcinogenesis* **31**(4): 745-750. DOI: 10.1093/carcin/bgq033  
959  
960 Cole, K. A., E. F. Attiyeh, Y. P. Mosse, M. J. Laquaglia, S. J. Diskin, G. M. Brodeur and  
961 J. M. Maris (2008). "A functional screen identifies miR-34a as a candidate  
962 neuroblastoma tumor suppressor gene." *Mol Cancer Res* **6**(5): 735-742. DOI:  
963 10.1158/1541-7786.MCR-07-2102  
964  
965 Conley, A. B. and I. K. Jordan (2012). "Epigenetic regulation of human cis-natural  
966 antisense transcripts." *Nucleic Acids Res* **40**(4): 1438-1445. DOI:  
967 10.1093/nar/gkr1010  
968  
969 Consortium, E. P. (2012). "An integrated encyclopedia of DNA elements in the  
970 human genome." *Nature* **489**(7414): 57-74. DOI: 10.1038/nature11247  
971  
972 Ding, N., H. Wu, T. Tao and E. Peng (2017). "NEAT1 regulates cell proliferation  
973 and apoptosis of ovarian cancer by miR-34a-5p/BCL2." *Onco Targets Ther* **10**:  
974 4905-4915. DOI: 10.2147/OTT.S142446  
975  
976 Djebali, S., C. A. Davis, A. Merkel, A. Dobin, T. Lassmann, A. Mortazavi, A. Tanzer, J.  
977 Lagarde, W. Lin, F. Schlesinger, C. Xue, G. K. Marinov, J. Khatun, B. A. Williams, C.  
978 Zaleski, J. Rozowsky, M. Roder, F. Kokocinski, R. F. Abdelhamid, T. Alioto, I.  
979 Antoshechkin, M. T. Baer, N. S. Bar, P. Batut, K. Bell, I. Bell, S. Chakrabortty, X.  
980 Chen, J. Chrast, J. Curado, T. Derrien, J. Drenkow, E. Dumais, J. Dumais, R.  
981 Duttagupta, E. Falconnet, M. Fastuca, K. Fejes-Toth, P. Ferreira, S. Foissac, M. J.  
982 Fullwood, H. Gao, D. Gonzalez, A. Gordon, H. Gunawardena, C. Howald, S. Jha, R.  
983 Johnson, P. Kapranov, B. King, C. Kingswood, O. J. Luo, E. Park, K. Persaud, J. B.  
984 Preall, P. Ribeca, B. Risk, D. Robyr, M. Sammeth, L. Schaffer, L. H. See, A. Shahab, J.  
985 Skancke, A. M. Suzuki, H. Takahashi, H. Tilgner, D. Trout, N. Walters, H. Wang, J.  
986 Wrobel, Y. Yu, X. Ruan, Y. Hayashizaki, J. Harrow, M. Gerstein, T. Hubbard, A.  
987 Reymond, S. E. Antonarakis, G. Hannon, M. C. Giddings, Y. Ruan, B. Wold, P.  
988 Carninci, R. Guigo and T. R. Gingeras (2012). "Landscape of transcription in  
989 human cells." *Nature* **489**(7414): 101-108. DOI: 10.1038/nature11233  
990

- 991 Gallardo, E., A. Navarro, N. Vinolas, R. M. Marrades, T. Diaz, B. Gel, A. Quera, E.  
992 Bandres, J. Garcia-Foncillas, J. Ramirez and M. Monzo (2009). "miR-34a as a  
993 prognostic marker of relapse in surgically resected non-small-cell lung cancer."  
994 Carcinogenesis **30**(11): 1903-1909. DOI: 10.1093/carcin/bgp219  
995
- 996 Geiger, T., A. Wehner, C. Schaab, J. Cox and M. Mann (2012). "Comparative  
997 proteomic analysis of eleven common cell lines reveals ubiquitous but varying  
998 expression of most proteins." Mol Cell Proteomics **11**(3): M111 014050. DOI:  
999 10.1074/mcp.M111.014050  
1000
- 1001 Granholm, V., S. Kim, J. C. Navarro, E. Sjolund, R. D. Smith and L. Kall (2014). "Fast  
1002 and accurate database searches with MS-GF+Percolator." J Proteome Res **13**(2):  
1003 890-897. DOI: 10.1021/pr400937n  
1004
- 1005 Grossman, R. L., A. P. Heath, V. Ferretti, H. E. Varmus, D. R. Lowy, W. A. Kibbe and  
1006 L. M. Staudt (2016). "Toward a Shared Vision for Cancer Genomic Data." N Engl J  
1007 Med **375**(12): 1109-1112. DOI: 10.1056/NEJMp1607591  
1008
- 1009 Holman, J. D., D. L. Tabb and P. Mallick (2014). "Employing ProteoWizard to  
1010 Convert Raw Mass Spectrometry Data." Curr Protoc Bioinformatics **46**: 13 24 11-  
1011 19. DOI: 10.1002/0471250953.bi1324s46  
1012
- 1013 Hung, T., Y. Wang, M. F. Lin, A. K. Koegel, Y. Kotake, G. D. Grant, H. M. Horlings, N.  
1014 Shah, C. Umbricht, P. Wang, Y. Wang, B. Kong, A. Langerod, A. L. Borresen-Dale, S.  
1015 K. Kim, M. van de Vijver, S. Sukumar, M. L. Whitfield, M. Kellis, Y. Xiong, D. J. Wong  
1016 and H. Y. Chang (2011). "Extensive and coordinated transcription of noncoding  
1017 RNAs within cell-cycle promoters." Nat Genet **43**(7): 621-629. DOI:  
1018 10.1038/ng.848  
1019
- 1020 Hunten, S., M. Kaller, F. Drepper, S. Oeljeklaus, T. Bonfert, F. Erhard, A. Dueck, N.  
1021 Eichner, C. C. Friedel, G. Meister, R. Zimmer, B. Warscheid and H. Hermeking  
1022 (2015). "p53-Regulated Networks of Protein, mRNA, miRNA, and lncRNA  
1023 Expression Revealed by Integrated Pulsed Stable Isotope Labeling With Amino  
1024 Acids in Cell Culture (pSILAC) and Next Generation Sequencing (NGS) Analyses."  
1025 Mol Cell Proteomics **14**(10): 2609-2629. DOI: 10.1074/mcp.M115.050237  
1026
- 1027 International Human Genome Sequencing, C. (2004). "Finishing the euchromatic  
1028 sequence of the human genome." Nature **431**(7011): 931-945. DOI:  
1029 10.1038/nature03001  
1030
- 1031 Johnsson, P., A. Ackley, L. Vidarsdottir, W. O. Lui, M. Corcoran, D. Grander and K.  
1032 V. Morris (2013). "A pseudogene long-noncoding-RNA network regulates PTEN  
1033 transcription and translation in human cells." Nat Struct Mol Biol **20**(4): 440-  
1034 446. DOI: 10.1038/nsmb.2516  
1035
- 1036 Katayama, S., Y. Tomaru, T. Kasukawa, K. Waki, M. Nakanishi, M. Nakamura, H.  
1037 Nishida, C. C. Yap, M. Suzuki, J. Kawai, H. Suzuki, P. Carninci, Y. Hayashizaki, C.  
1038 Wells, M. Frith, T. Ravasi, K. C. Pang, J. Hallinan, J. Mattick, D. A. Hume, L. Lipovich,  
1039 S. Batalov, P. G. Engstrom, Y. Mizuno, M. A. Faghihi, A. Sandelin, A. M. Chalk, S.

- 1040 Mottagui-Tabar, Z. Liang, B. Lenhard, C. Wahlestedt, R. G. E. R. Group, G. Genome  
1041 Science and F. Consortium (2005). "Antisense transcription in the mammalian  
1042 transcriptome." *Science* **309**(5740): 1564-1566. DOI: 10.1126/science.1112009
- 1043
- 1044 Kent, W. J., C. W. Sugnet, T. S. Furey, K. M. Roskin, T. H. Pringle, A. M. Zahler and D.  
1045 Haussler (2002). "The human genome browser at UCSC." *Genome Res* **12**(6):  
1046 996-1006. DOI: 10.1101/gr.229102. Article published online before print in May  
1047 2002
- 1048
- 1049 Kim, K. H., H. J. Kim and T. R. Lee (2017). "Epidermal long non-coding RNAs are  
1050 regulated by ultraviolet irradiation." *Gene* **637**: 196-202. DOI:  
1051 10.1016/j.gene.2017.09.043
- 1052
- 1053 Kim, S. and P. A. Pevzner (2014). "MS-GF+ makes progress towards a universal  
1054 database search tool for proteomics." *Nature Communications* **5**: 5277. DOI:  
1055 10.1038/ncomms6277
- 1056
- 1057 Kong, L., Y. Zhang, Z. Q. Ye, X. Q. Liu, S. Q. Zhao, L. Wei and G. Gao (2007). "CPC:  
1058 assess the protein-coding potential of transcripts using sequence features and  
1059 support vector machine." *Nucleic Acids Res* **35**(Web Server issue): W345-349.  
1060 DOI: 10.1093/nar/gkm391
- 1061
- 1062 Lal, A., M. P. Thomas, G. Altschuler, F. Navarro, E. O'Day, X. L. Li, C. Concepcion, Y.  
1063 C. Han, J. Thiery, D. K. Rajani, A. Deutsch, O. Hofmann, A. Ventura, W. Hide and J.  
1064 Lieberman (2011). "Capture of microRNA-bound mRNAs identifies the tumor  
1065 suppressor miR-34a as a regulator of growth factor signaling." *PLoS Genet* **7**(11):  
1066 e1002363. DOI: 10.1371/journal.pgen.1002363
- 1067
- 1068 Leveille, N., C. A. Melo, K. Rooijers, A. Diaz-Lagares, S. A. Melo, G. Korkmaz, R.  
1069 Lopes, F. Akbari Moqadam, A. R. Maia, P. J. Wijchers, G. Geeven, M. L. den Boer, R.  
1070 Kalluri, W. de Laat, M. Esteller and R. Agami (2015). "Genome-wide profiling of  
1071 p53-regulated enhancer RNAs uncovers a subset of enhancers controlled by a  
1072 lncRNA." *Nature Communications* **6**: 6520. DOI: 10.1038/ncomms7520
- 1073
- 1074 Liu, C., K. Kelnar, B. Liu, X. Chen, T. Calhoun-Davis, H. Li, L. Patrawala, H. Yan, C.  
1075 Jeter, S. Honorio, J. F. Wiggins, A. G. Bader, R. Fagin, D. Brown and D. G. Tang  
1076 (2011). "The microRNA miR-34a inhibits prostate cancer stem cells and  
1077 metastasis by directly repressing CD44." *Nat Med* **17**(2): 211-215. DOI:  
1078 10.1038/nm.2284
- 1079
- 1080 Memczak, S., M. Jens, A. Elefsinioti, F. Torti, J. Krueger, A. Rybak, L. Maier, S. D.  
1081 Mackowiak, L. H. Gregersen, M. Munschauer, A. Loewer, U. Ziebold, M.  
1082 Landthaler, C. Kocks, F. le Noble and N. Rajewsky (2013). "Circular RNAs are a  
1083 large class of animal RNAs with regulatory potency." *Nature* **495**(7441): 333-  
1084 338. DOI: 10.1038/nature11928
- 1085
- 1086 Ng, S. Y., G. K. Bogu, B. S. Soh and L. W. Stanton (2013). "The long noncoding RNA  
1087 RMST interacts with SOX2 to regulate neurogenesis." *Mol Cell* **51**(3): 349-359.  
1088 DOI: 10.1016/j.molcel.2013.07.017

- 1089  
1090 Ng, S. Y., R. Johnson and L. W. Stanton (2012). "Human long non-coding RNAs  
1091 promote pluripotency and neuronal differentiation by association with  
1092 chromatin modifiers and transcription factors." *EMBO J* **31**(3): 522-533. DOI:  
1093 10.1038/emboj.2011.459
- 1094  
1095 O'Leary, N. A., M. W. Wright, J. R. Brister, S. Ciufo, D. Haddad, R. McVeigh, B.  
1096 Rajput, B. Robbertse, B. Smith-White, D. Ako-Adjei, A. Astashyn, A. Badretdin, Y.  
1097 Bao, O. Blinkova, V. Brover, V. Chetvernin, J. Choi, E. Cox, O. Ermolaeva, C. M.  
1098 Farrell, T. Goldfarb, T. Gupta, D. Haft, E. Hatcher, W. Hlavina, V. S. Joardar, V. K.  
1099 Kodali, W. Li, D. Maglott, P. Masterson, K. M. McGarvey, M. R. Murphy, K. O'Neill,  
1100 S. Pujar, S. H. Rangwala, D. Rausch, L. D. Riddick, C. Schoch, A. Shkeda, S. S. Storz,  
1101 H. Sun, F. Thibaud-Nissen, I. Tolstoy, R. E. Tully, A. R. Vatsan, C. Wallin, D. Webb,  
1102 W. Wu, M. J. Landrum, A. Kimchi, T. Tatusova, M. DiCuccio, P. Kitts, T. D. Murphy  
1103 and K. D. Pruitt (2016). "Reference sequence (RefSeq) database at NCBI: current  
1104 status, taxonomic expansion, and functional annotation." *Nucleic Acids Res*  
1105 **44**(D1): D733-745. DOI: 10.1093/nar/gkv1189
- 1106  
1107 Ozsolak, F., P. Kapranov, S. Foissac, S. W. Kim, E. Fishilevich, A. P. Monaghan, B.  
1108 John and P. M. Milos (2010). "Comprehensive polyadenylation site maps in yeast  
1109 and human reveal pervasive alternative polyadenylation." *Cell* **143**(6): 1018-  
1110 1029. DOI: 10.1016/j.cell.2010.11.020
- 1111  
1112 Polson, A., E. Durrett and D. Reisman (2011). "A bidirectional promoter reporter  
1113 vector for the analysis of the p53/WDR79 dual regulatory element." *Plasmid*  
1114 **66**(3): 169-179. DOI: 10.1016/j.plasmid.2011.08.004
- 1115  
1116 Rashi-Elkeles, S., H. J. Warnatz, R. Elkon, A. Kupershtain, Y. Chobod, A. Paz, V.  
1117 Amstislavskiy, M. Sultan, H. Safer, W. Nietfeld, H. Lehrach, R. Shamir, M. L. Yaspo  
1118 and Y. Shiloh (2014). "Parallel profiling of the transcriptome, cistrome, and  
1119 epigenome in the cellular response to ionizing radiation." *Sci Signal* **7**(325): rs3.  
1120 DOI: 10.1126/scisignal.2005032
- 1121  
1122 Raver-Shapira, N., E. Marciano, E. Meiri, Y. Spector, N. Rosenfeld, N. Moskovits, Z.  
1123 Bentwich and M. Oren (2007). "Transcriptional activation of miR-34a  
1124 contributes to p53-mediated apoptosis." *Mol Cell* **26**(5): 731-743. DOI:  
1125 10.1016/j.molcel.2007.05.017
- 1126  
1127 Rinn, J. L., M. Kertesz, J. K. Wang, S. L. Squazzo, X. Xu, S. A. Brugmann, L. H.  
1128 Goodnough, J. A. Helms, P. J. Farnham, E. Segal and H. Y. Chang (2007).  
1129 "Functional demarcation of active and silent chromatin domains in human HOX  
1130 loci by noncoding RNAs." *Cell* **129**(7): 1311-1323. DOI:  
1131 10.1016/j.cell.2007.05.022
- 1132  
1133 Rokavec, M., M. G. Oner, H. Li, R. Jackstadt, L. Jiang, D. Lodygin, M. Kaller, D. Horst,  
1134 P. K. Ziegler, S. Schwitalla, J. Slotta-Huspenina, F. G. Bader, F. R. Greten and H.  
1135 Hermeking (2015). "Corrigendum. IL-6R/STAT3/miR-34a feedback loop  
1136 promotes EMT-mediated colorectal cancer invasion and metastasis." *J Clin Invest*  
1137 **125**(3): 1362. DOI: 10.1172/JCI81340

- 1138  
1139 Schneider, C. A., W. S. Rasband and K. W. Eliceiri (2012). "NIH Image to ImageJ:  
1140 25 years of image analysis." *Nat Methods* **9**(7): 671-675.  
1141  
1142 Serviss, J. T. (2017). miR34AasRNAproject.  
1143 [https://github.com/GranderLab/miR34a\\_asRNA\\_project](https://github.com/GranderLab/miR34a_asRNA_project)  
1144  
1145 Serviss, J. T., P. Johnsson and D. Grander (2014). "An emerging role for long non-  
1146 coding RNAs in cancer metastasis." *Front Genet* **5**: 234. DOI:  
1147 10.3389/fgene.2014.00234  
1148  
1149 Slabakova, E., Z. Culig, J. Remsik and K. Soucek (2017). "Alternative mechanisms  
1150 of miR-34a regulation in cancer." *Cell Death Dis* **8**(10): e3100. DOI:  
1151 10.1038/cddis.2017.495  
1152  
1153 Stahlhut, C. and F. J. Slack (2015). "Combinatorial Action of MicroRNAs let-7 and  
1154 miR-34 Effectively Synergizes with Erlotinib to Suppress Non-small Cell Lung  
1155 Cancer Cell Proliferation." *Cell Cycle* **14**(13): 2171-2180. DOI:  
1156 10.1080/15384101.2014.1003008  
1157  
1158 Su, X., D. Chakravarti, M. S. Cho, L. Liu, Y. J. Gi, Y. L. Lin, M. L. Leung, A. El-Naggar,  
1159 C. J. Creighton, M. B. Suraokar, I. Wistuba and E. R. Flores (2010). "TAp63  
1160 suppresses metastasis through coordinate regulation of Dicer and miRNAs."  
1161 *Nature* **467**(7318): 986-990. DOI: 10.1038/nature09459  
1162  
1163 Sun, F., H. Fu, Q. Liu, Y. Tie, J. Zhu, R. Xing, Z. Sun and X. Zheng (2008).  
1164 "Downregulation of CCND1 and CDK6 by miR-34a induces cell cycle arrest."  
1165 *FEBS Lett* **582**(10): 1564-1568. DOI: 10.1016/j.febslet.2008.03.057  
1166  
1167 Tarasov, V., P. Jung, B. Verdoodt, D. Lodygin, A. Epanchintsev, A. Menssen, G.  
1168 Meister and H. Hermeking (2007). "Differential regulation of microRNAs by p53  
1169 revealed by massively parallel sequencing: miR-34a is a p53 target that induces  
1170 apoptosis and G1-arrest." *Cell Cycle* **6**(13): 1586-1593. DOI:  
1171 10.4161/cc.6.13.4436  
1172  
1173 Team, R. C. (2017). "R: A Language and Environment for Statistical Computing."  
1174 from <https://www.R-project.org/>.  
1175  
1176 Therneau, T. M. (2015). A Package for Survival Analysis in S. version 2.38.  
1177 <https://CRAN.R-project.org/package=survival>  
1178  
1179 Turner, A. M., A. M. Ackley, M. A. Matrone and K. V. Morris (2012).  
1180 "Characterization of an HIV-targeted transcriptional gene-silencing RNA in  
1181 primary cells." *Hum Gene Ther* **23**(5): 473-483. DOI: 10.1089/hum.2011.165  
1182  
1183 Vogt, M., J. Mundig, M. Gruner, S. T. Liffers, B. Verdoodt, J. Hauk, L.  
1184 Steinstraesser, A. Tannapfel and H. Hermeking (2011). "Frequent concomitant  
1185 inactivation of miR-34a and miR-34b/c by CpG methylation in colorectal,  
1186 pancreatic, mammary, ovarian, urothelial, and renal cell carcinomas and soft

1187 tissue sarcomas." *Virchows Arch* **458**(3): 313-322. DOI: 10.1007/s00428-010-  
1188 1030-5  
1189  
1190 Wang, L., P. Bu, Y. Ai, T. Srinivasan, H. J. Chen, K. Xiang, S. M. Lipkin and X. Shen  
1191 (2016). "A long non-coding RNA targets microRNA miR-34a to regulate colon  
1192 cancer stem cell asymmetric division." *eLife* **5**. DOI: 10.7554/eLife.14620  
1193  
1194 Wang, L., H. J. Park, S. Dasari, S. Wang, J. P. Kocher and W. Li (2013). "CPAT:  
1195 Coding-Potential Assessment Tool using an alignment-free logistic regression  
1196 model." *Nucleic Acids Res* **41**(6): e74. DOI: 10.1093/nar/gkt006  
1197  
1198 Wang, X., J. Li, K. Dong, F. Lin, M. Long, Y. Ouyang, J. Wei, X. Chen, Y. Weng, T. He  
1199 and H. Zhang (2015). "Tumor suppressor miR-34a targets PD-L1 and functions  
1200 as a potential immunotherapeutic target in acute myeloid leukemia." *Cell Signal*  
1201 **27**(3): 443-452. DOI: 10.1016/j.cellsig.2014.12.003  
1202  
1203 Wickham, H. (2016). gtable: Arrange 'Grobs' in Tables. R package version 0.2.0.  
1204 <https://CRAN.R-project.org/package=gtable>  
1205  
1206 Wickham, H. (2017). scales: Scale Functions for Visualization. R package version  
1207 0.5.0. <https://CRAN.R-project.org/package=scales>  
1208  
1209 Wickham, H. (2017). tidyverse: Easily Install and Load the 'Tidyverse'. R package  
1210 version 1.2.1. <https://CRAN.R-project.org/package=tidyverse>  
1211  
1212 Wickham, L. H. a. H. (2017). rlang: Functions for Base Types and Core R and  
1213 'Tidyverse' Features. R package version 0.1.4. [https://CRAN.R-  
1214 project.org/package=rlang](https://CRAN.R-project.org/package=rlang)  
1215  
1216 Wickham, S. M. B. a. H. (2014). magrittr: A Forward-Pipe Operator for R. R  
1217 package version 1.5. <https://CRAN.R-project.org/package=magrittr>  
1218  
1219 Wilkins, D. ggenes: Draw Gene Arrow Maps in 'ggplot2'. R package version  
1220 0.2.0.9003. <https://github.com/wilkox/ggenes>  
1221  
1222 Xiao, N. (2017). liftr: Containerize R Markdown Documents. R package version  
1223 0.7. <https://CRAN.R-project.org/package=liftr>  
1224  
1225 Xie, Y. (2017). knitr: A General-Purpose Package for Dynamic Report Generation  
1226 in R. R package version 1.17. <https://yihui.name/knitr/>  
1227  
1228 Yang, P., Q. J. Li, Y. Feng, Y. Zhang, G. J. Markowitz, S. Ning, Y. Deng, J. Zhao, S.  
1229 Jiang, Y. Yuan, H. Y. Wang, S. Q. Cheng, D. Xie and X. F. Wang (2012). "TGF-beta-  
1230 miR-34a-CCL22 signaling-induced Treg cell recruitment promotes venous  
1231 metastases of HBV-positive hepatocellular carcinoma." *Cancer Cell* **22**(3): 291-  
1232 303. DOI: 10.1016/j.ccr.2012.07.023  
1233  
1234 Yap, K. L., S. Li, A. M. Munoz-Cabello, S. Raguz, L. Zeng, S. Mujtaba, J. Gil, M. J.  
1235 Walsh and M. M. Zhou (2010). "Molecular interplay of the noncoding RNA ANRIL

1236 and methylated histone H3 lysine 27 by polycomb CBX7 in transcriptional  
1237 silencing of INK4a." Mol Cell **38**(5): 662-674. DOI: 10.1016/j.molcel.2010.03.021  
1238  
1239 Yu, W., D. Gius, P. Onyango, K. Muldoon-Jacobs, J. Karp, A. P. Feinberg and H. Cui  
1240 (2008). "Epigenetic silencing of tumour suppressor gene p15 by its antisense  
1241 RNA." Nature **451**(7175): 202-206. DOI: 10.1038/nature06468  
1242  
1243 Zenz, T., J. Mohr, E. Eldering, A. P. Kater, A. Buhler, D. Kienle, D. Winkler, J. Durig,  
1244 M. H. van Oers, D. Mertens, H. Dohner and S. Stilgenbauer (2009). "miR-34a as  
1245 part of the resistance network in chronic lymphocytic leukemia." Blood **113**(16):  
1246 3801-3808. DOI: 10.1182/blood-2008-08-172254  
1247  
1248  
1249  
1250